(Wiedenkeller & Sharp 1984). TMB-8 (1 mM) was locally administered through the dialysis probe and ouabain-induced NA response was measured. A similar pharmacological intervention was performed and ouabain-induced ACh responses were measured. Sixty minutes after starting local administration of verapamil (100 μM), or ω-conotoxin GVIA (10 μM), ω-conotoxin MVIIC (10 μM), we measured the ouabain-induced ACh response. The inhibitor of membrane Na^+/Ca^{2+} exchange (KB7943; 10 μM) was locally administered through the dialysis probe and the ouabain-induced ACh response was measured. Third, an intracellular Ca^{2+} antagonist (TMB-8, 1 mM) was locally administered through the dialysis probe and ouabain-induced ACh response was measured.

Analytical procedure

Dialysate NA concentrations were measured by HPLC with electrochemical detection (HPLC-ECD; Eicom, Kyoto, Japan). An alumina procedure was performed to remove the interfering compounds from the dialysate. The detection limit was 50 fmol per injection. Dialysate ACh concentration was measured directly by another HPLC-ECD. The detection limit was 50 fmol per injection. Details of HPLC-ECD for the NA and ACh measurements have been described elsewhere (Akiyama *et al.* 1991, 1994).

At the end of each experiment, the cats were killed with an overdose of pentobarbital sodium, and the implant sites were checked to confirm that the dialysis probes had been implanted within the left ventricular myocardium. Statistical analysis of the data was performed by analysis of variance (ANOVA). Statistical significance was defined as $P < 0.05$. Values are presented as mean ± SE.

Results

Protocol 1: Time course of dialysate NA and ACh levels during local administration of ouabain

Although local administration of ouabain did not affect haemodynamic parameters including heart rate, mean arterial pressure and electrocardiogram, ouabain induced the efflux of NA. Figure 1 (upper panel) shows the time course of the dialysate NA levels during local administration of ouabain (100 μM). Dialysate NA level increased significantly from 0.18 ± 0.06 nmol L^{-1} at control to 2.39 ± 0.53 nmol L^{-1} at 10, 12.92 ± 1.39 nmol L^{-1} at 20 min and 14.79 ± 1.97 nmol L^{-1} at 30 min. Subsequently, a slow decline occurred but high dialysate NA levels were maintained during locally applied ouabain. Peak level of dialysate NA ranged from 20 to 30 min after the beginning of ouabain administration. Figure 1 (lower panel) shows the time course of the dialysate ACh levels during local administration of ouabain (100 μM). Dialysate ACh level increased significantly from 0.91 ± 0.05 nmol at control to 3.6 ± 0.60 nmol L^{-1} at 0–15, 8.1 ± 1.4 nmol L^{-1} at 15–30 min and 6.8 ± 1.25 nmol L^{-1} at 30–45 min. Peak level of dialysate ACh appeared at 15–30 min after the beginning of ouabain administration.

Protocol 2: Influence of denervation and TTX on dialysate NA and ACh responses evoked by ouabain

We sampled the dialysates over 60 min of ouabain administration. To compare ouabain-induced NA or ACh levels under various interventions, ouabain-induced dialysate NA or ACh levels were subtracted from the control values. The sum of relative changes in dialysate NA or ACh (the unit: Σnmol/L) was expressed as an index of total NA or ACh release evoked by ouabain. Figure 2 (upper panel) shows the total NA release evoked by ouabain when cardiac sympathetic nerves were either intact, transected, pretreated with TTX. The ouabain-induced total NA release did not differ among them. Figure 2 (lower panel) shows the total ACh release evoked by ouabain when cardiac parasympathetic nerves were either intact, transected, or pretreated with TTX. The ouabain-induced total ACh release did not differ between the intact cardiac parasympathetic nerve and denervated groups whereas addition of TTX significantly inhibited the total ACh release by approx. 57% of vehicle.

Protocol 3: Influence of transport blocking agents on dialysate NA and ACh responses evoked by ouabain

Figure 3 (upper panel) shows the total NA release evoked by ouabain among various pharmacological interventions. Pretreatment with reserpine caused significant augmentation of the ouabain-induced total NA release whereas pretreatment with desipramine caused significant suppression of the total NA release. Figure 3 (lower panel) shows the total ACh release evoked by ouabain among various pharmacological interventions. The ouabain-induced total ACh release did not differ between the intact and hemicholinium-3 pretreated groups whereas addition of vesamicol significantly inhibited the total ACh release by approx. 45% of vehicle.

Protocol 4: Influence of Ca^{2+} mobilization on dialysate NA and ACh responses evoked by ouabain

Figure 4 (upper panel) shows the total NA release evoked by ouabain among various Ca^{2+} interventions. The total NA release in the 60 min after administration

Journal compilation © 2007 Scandinavian Physiological Society, doi: 10.1111/j.1748-1716.2007.01749.x

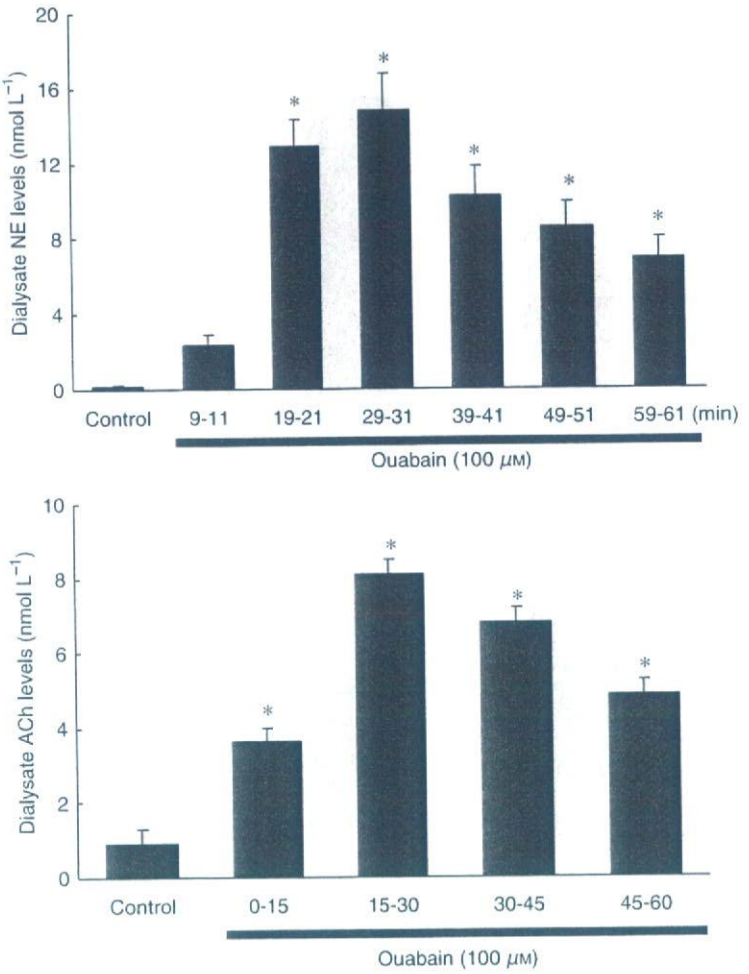

Figure 1 Upper panel: Time course of dialysate noradrenaline (NA) levels during local administration of ouabain (100 μM). Ouabain increased the dialysate NA levels. Subsequently, a slow decline occurred but high NA levels were maintained. Lower panel: Time course of dialysate acetylcholine (ACh) levels during local administration of ouabain (100 μM). Ouabain increased the dialysate ACh levels. Subsequently, a slow decline occurred but high ACh levels were maintained. Values are presented as the mean ± SE (for each column $n = 6$) $^*P < 0.05$ vs. control.

of ouabain was significantly suppressed by approx. 47% and 55% of vehicle by addition of verapamil and ω-conotoxin GVIA. Pretreatment with TMB-8 caused significant suppression of the ouabain-induced total NA release whereas pretreatment with neither KB-7943 nor dechlorobezamil altered the total NA release. Figure 4 (lower panel) shows the total ACh release evoked by ouabain among various Ca^{2+} interventions. The total ACh release in the 60 min after administration of ouabain was significantly suppressed by approx. 57% of vehicle by addition of ω-conotoxin MVIIC. Pretreatment with neither verapamil nor ω-conotoxin GVIA altered the total ACh release. Pretreatment with TMB-8 caused significant suppression of the ouabain-induced total ACh release whereas pretreatment with KB-7943 did not alter the total ACh release.

Discussion

The present study indicates that in an *in vivo* preparation, ouabain alone induced NA or ACh release from sympathetic or parasympathetic nerve endings respectively. This discussion addresses mainly similarities and differences in ouabain alone induced NA or ACh releasing sites and mechanisms.

Regional depolarization evoked by ouabain

At the post-ganglionic nervous endings, ouabain induced NA and ACh release. The transection of sympathetic or parasympathetic nerve did not affect the amount of NA or ACh release evoked by ouabain. After the transection of cardiac sympathetic or parasympathetic nerves, ouabain at 100 μM induced increases in dialysate NA or ACh levels, which were as much as those evoked by electrical stimulation of the autonomic nerve (Akiyama *et al.* 1994, Yamazaki *et al.* 1997). These data suggest that ouabain itself induces regional depolarization following exocytosis. In the case of locally administered ouabain, ouabain produced intracellular Na^+ accumulation evoked by the inhibition of Na^+,K^+-ATPase (Mclvor & Cummings 1987).

 doi: 10.1111/j.1748-1716.2007.01749.x

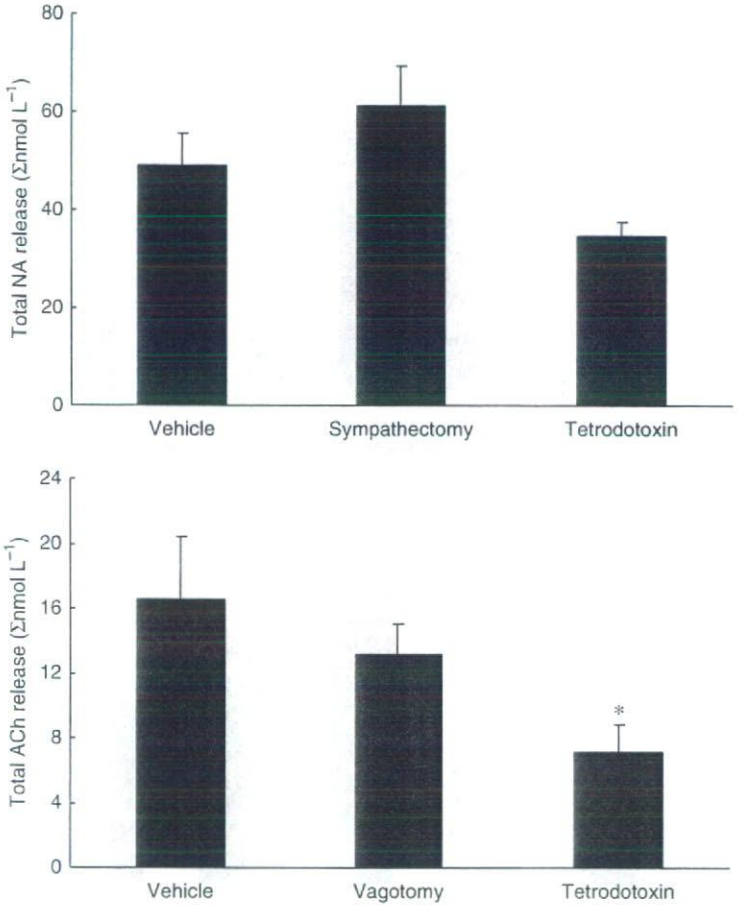

Figure 2 Upper panel: Ouabain-induced dialysate noradrenaline (NA) release in vehicle, cardiac sympathetic denervated and tetrodotoxin pretreated groups. Total NA release evoked by ouabain did not differ among the three groups. Lower panel: Ouabain-induced dialysate acetylcholine (ACh) release in vehicle, cardiac vagal denervated and tetrodotoxin pretreated groups. Total ACh release evoked by ouabain was suppressed by the pretreatment with tetrodotoxin. Values are presented as the mean ± SE (for each column $n = 6$). $^*P < 0.05$ vs. vehicle.

Regional depolarization may occur because of intracellular Na^+ accumulation (Calabresi *et al.* 1999, Dierkes *et al.* 2006). Similar finding was observed on motor endplate (Zemkova *et al.* 1990). Ouabain can increase the spontaneous ACh release by progressive decline in membrane potential when Na^+ pump is inhibited. If regional depolarization does indeed induce ACh or NA release via exocytosis from the stored vesicle, then pretreatment with TTX could inhibit this response. Local administration of TTX markedly inhibits ACh release whereas it only slightly inhibits the NA release evoked by ouabain. These results indicate that ouabain caused regional depolarization and exocytotic ACh release at the parasympathetic nerve endings. This conclusion is consistent with *in vitro* studies reported by Satoh & Nakazato (1992), and raises the question as to why TTX inhibited the ACh release but not the NA release evoked by ouabain. In the case of NA efflux evoked by ouabain, intracellular Na^+ accumulation may lead to a reduction in the Na^+ gradient between the intracellular and extracellular spaces. This reduced Na^+ gradient may cause carrier-mediated outward NA transport from axoplasma (Sharma *et al.* 1980). The threshold for intracellular Na^+ accumulation coupled to carrier-mediated outward NA transport might be lower than that for regional depolarization. Thus Na^+ accumulation coupled to regional depolarization may occur at the parasympathetic nerve endings but not at the sympathetic nerve endings.

The sites of neurotransmitter efflux evoked by ouabain

In general, two possible sites (the stored vesicle and axoplasma) were proposed to derive efflux of neurotransmitter at the nerve endings (Smith 1992, Vizi 1998). In the cholinergic nerve endings, a quantum amount of ACh was released from the stored vesicle via depolarization. Furthermore, a non-quantum amount of ACh seems to be leaked from the axoplasma without ACh transporter (Nikolsky *et al.* 1991). Local administration of vesamicol suppressed the ACh efflux evoked by ouabain. In contrast, local administration of hemicholinium-3 did not affect the ACh efflux evoked by ouabain. These data suggested that the ACh efflux was predominantly derived from the stored vesicle. This finding is consistent with the above-mentioned

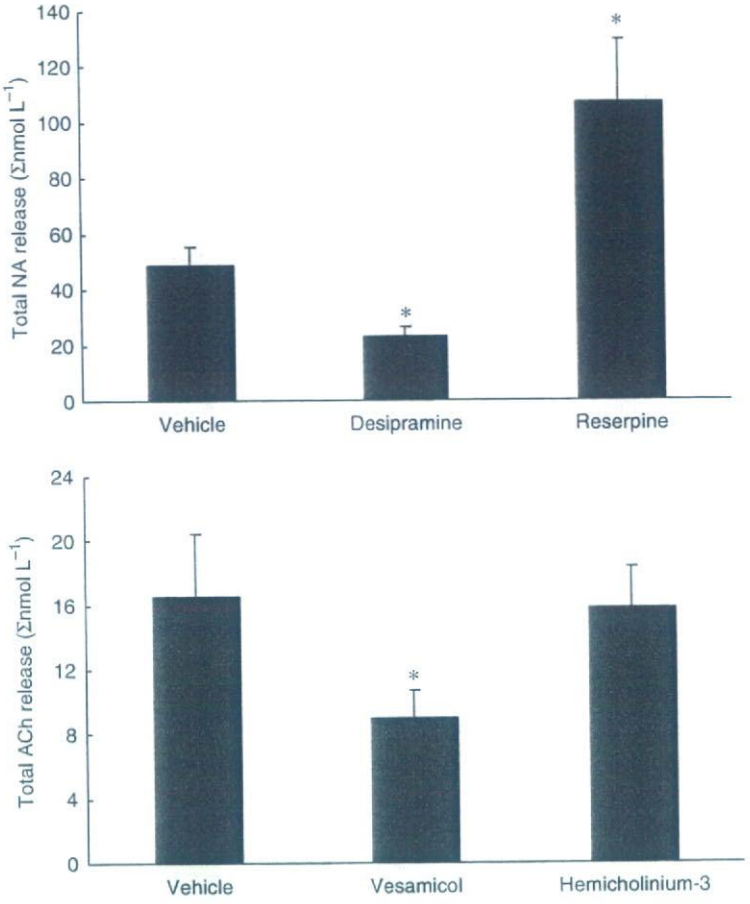

Figure 3 Upper panel: Ouabain-induced dialysate noradrenaline (NA) release among vehicle, desipramine and reserpine pretreated groups. Total NA release evoked by ouabain was suppressed by the pretreatment with desipramine and augmented by that with reserpine. Lower panel: Ouabain-induced dialysate acetylcholine (ACh) release in vehicle, vesamicol and hemicholinium-3 pretreated groups. Total ACh release evoked by ouabain was suppressed by the pretreatment with vesamicol. Values are presented as the mean ± SE (for each column $n = 6$). $^*P < 0.05$ vs. vehicle.

mechanism. Our data did not rule out the possibility of ACh efflux from the axoplasma. Vesamicol lowered the non-quantum ACh release by blocking the incorporated vesicle transporter in the terminal membrane (Edward *et al.* 1985). This involvement seems to be smaller than the involvement of ACh efflux from the stored vesicle.

Previous studies suggested that two different mechanisms (exocytosis and carrier-mediated outward transport) contributed to the amount of NA efflux evoked by ouabain (Kranzhöfer *et al.* 1991, Haass *et al.* 1997). The exocytotic NA release derived from the stored vesicle, whereas NA transporter carried out NA from the axoplasmic site via a reduced Na^+ gradient. However, it is uncertain which mechanism is predominantly involved in ouabain-induced NA efflux. To examine which site predominantly induced the neurotransmitter efflux evoked by ouabain, we administered vesicle and membranous amine transport blockers, which affected the neurotransmitter efflux evoked by ouabain. If NA efflux predominantly derives from the axoplasmic site, reserpine could increase axoplasmic NA level and augment the outward NA transport evoked by ouabain. Furthermore, as desipramine impairs carrier-mediated NA transport in both directions, desipramine could block NA efflux. NA release evoked by ouabain was augmented by local administration of reserpine but suppressed by desipramine. These data support the contention that ouabain-induced NA efflux is predominantly derived from the axoplasmic site.

Involvement of Ca^{2+} on ouabain-induced neurotransmitter efflux

Most *in vitro* studies suggested that ouabain somehow increases intracellular Ca^{2+} levels at the nerve endings and synaptosomes (Katsuragi *et al.* 1994, Casali *et al.* 1995, Wasserstrom & Aistrup 2005). Ouabain-induced intracellular Na^+ accumulation could evoke an elevation of intracellular Ca^{2+} level via Ca^{2+} channel opening (Katsuragi *et al.* 1994), Ca^{2+} release from internal stores (Nishio *et al.* 2004), and/or Na^+/Ca^{2+} exchange (Verbny *et al.* 2002). Thus, the elevation of intracellular Ca^{2+} may be associated with NA or ACh release from the autonomic nerve endings. At the parasympathetic nerve endings, neither verapamil nor ω-conotoxin GVIA

 doi: 10.1111/j.1748-1716.2007.01749.x

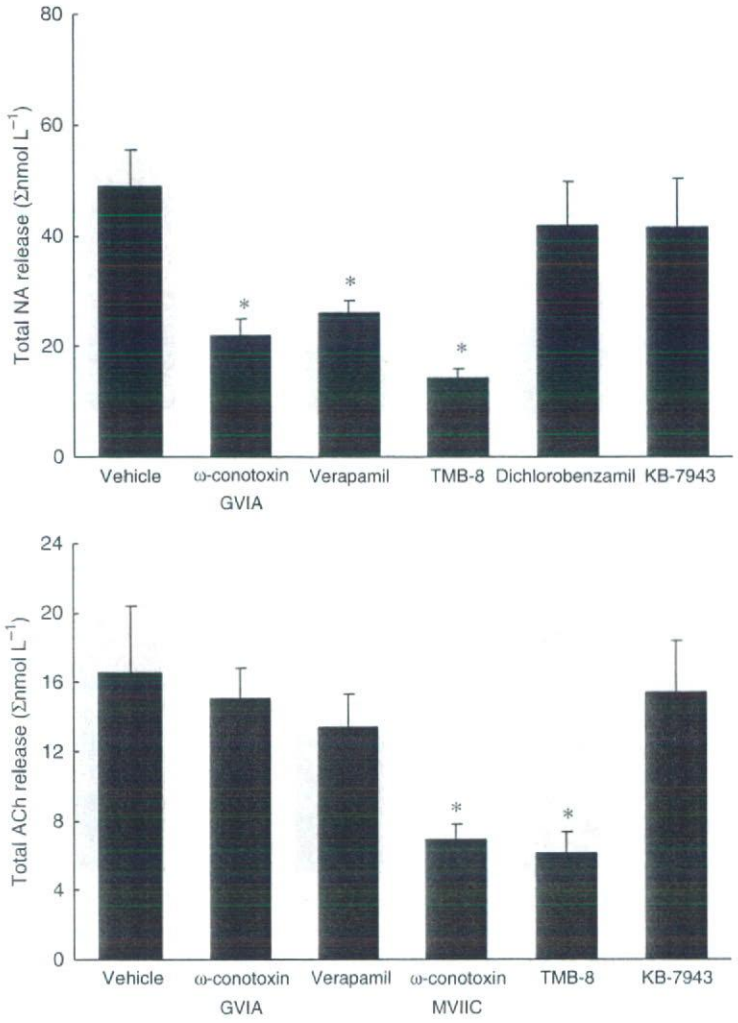

Figure 4 Upper panel: Ouabain-induced dialysate noradrenaline (NA) release in various Ca^{2+} interventions. Total NA release evoked by ouabain was suppressed by the pretreatment with ω-conotoxin GVIA, verapamil, TMB-8. Lower panel: Ouabain-induced dialysate acetylcholine (ACh) release in various Ca^{2+} interventions. Total ACh release evoked by ouabain was suppressed by the pretreatment with ω-conotoxin MVIICA or TMB-8. Values are presented as the mean ± SE (for each column $n = 6$). $^*P < 0.05$ vs. vehicle.

affected ACh release but ω-conotoxin MVIIC inhibited ACh release evoked by ouabain. Furthermore, KB-7943 did not affect either the ACh release evoked by ouabain. These data suggest that N or L-type Ca^{2+} channels or reversal Na^+/Ca^{2+} exchange might not be responsible for the ACh release evoked by ouabain. However, a marked suppression of ouabain-induced ACh release was observed with the addition of P/Q types channel blocker or TMB-8. In the case of parasympathetic nerve endings, Ca^{2+} elevation coupled to ACh release might be derived via internal stores or Ca^{2+} channels (P/Q types) rather than Na^+/Ca^{2+} exchange (Casali *et al.* 1995, Kawada *et al.* (in press)).

In the case of NA, ω-conotoxin GVIA or verapamil suppressed the NA release evoked by ouabain. Ouabain-induced NA release was independent of depolarization (TTX-resistant) but associated with the opening of Ca^{2+} channel. Furthermore, neither KB-7493 nor dichlorobenzamil affected the NA release evoked by ouabain. These data suggest that bi-directions of Na^+/Ca^{2+} exchange might not be responsible for the elevation of intracellular Ca^{2+} levels evoked by ouabain. A marked suppression of ouabain-induced NA release was observed with the addition of TMB-8. Taking these findings together, in the case of sympathetic nerve endings, Ca^{2+} elevation coupled to NA release might be derived via Ca^{2+} channels or internal store rather than membrane Na/Ca^{2+} exchange.

Although the type of Ca^{2+} channel for the NA or ACh release differed, involvement of cytosol Ca^{2+} in ouabain-induced neurotransmitter release did not differ between the parasympathetic and sympathetic nerve endings. However, the relation between TTX sensitive Na^+ channel and Ca^{2+} channel opening may differ between the parasympathetic and sympathetic nerve endings. In the present study, ouabain-induced NA efflux was suppressed by ω-conotoxin GVIA but not by TTX, indicating that TTX sensitive depolarization was not involved in Ca^{2+} channel opening coupled to exocytotic NA release. In contrast to NA release,

Journal compilation © 2007 Scandinavian Physiological Society, doi: 10.1111/j.1748-1716.2007.01749.x

ouabain-induced ACh release was suppressed by TTX and ω-conotoxin MVIIC, indicating that ouabain-induced depolarization and subsequently ACh release via P/Q type Ca^{2+} channel opening. TTX sensitive or resistant response may be interpreted as two different types of neurotransmitter release mechanisms. Alternatively, ouabain may have induced increases in intraneuronal Na^+ accumulation and elevation of extraneuronal K^+ levels by inhibition of Na^+,K^+-ATPase (D'Ambrosio *et al.* 2002). Elevations of both intracellular Na^+ and extracellular K^+ exerted regional depolarization following exocytosis via different mechanisms. In the previous study, we demonstrated that high K^+-induced NA release was insensitive to TTX but sensitive to ω-conotoxin GVIA. Furthermore, high K^+ caused a marked increase in dialysate NA but little increase in dialysate Ach (Yamazaki *et al.* 1998, Kawada *et al.* 2001). Thus high K^+-induced neurotransmitter release might greatly contribute to the increase in dialysate NA evoked by ouabain but might contribute little to the increase in dialysate ACh.

In conclusion, ouabain alone causes a brisk efflux of NA and ACh from cardiac sympathetic and parasympathetic nerve endings respectively. The ouabain-induced ACh release contributes to the mechanism of ACh exocytosis, which is triggered by centrally mediated or regional depolarization. The regional exocytosis is caused by opening of P/Q type Ca^{2+} channels and/or intracellular Ca^{2+} mobilization from the stored ACh vesicle. The ouabain-induced NA release contributes to the mechanisms of regional exocytosis and/or carrier-mediated outward transport of NA, from stored NA vesicle and/or axoplasma respectively. The regional exocytosis is caused by opening of N type Ca^{2+} channels and intracellular Ca^{2+} mobilization.

Conflict of interest

None.

This work was supported by Grants-in-Aid for scientific research (17591659) from the Ministry of Education, Culture, Sports, Science and Technology.

References

Akiyama, T., Yamazaki, T. & Ninomiya, I. 1991. *In vivo* monitoring of myocardial interstitial norepinephrine by dialysis technique. *Am J Physiol* **261**, H1643–H1647.

Akiyama, T., Yamazaki, T. & Ninomiya, I. 1994. *In vivo* detection of endogenous acetylcholine release in cat ventricles. *Am J Physiol* **266**, H854–H860.

Calabresi, P., Marfia, G.A., Centonze, D., Pisani, A. & Bernardi, G. 1999. Sodium influx plays a major role in the membrane depolarization induced by oxygen and glucose deprivation in rat striatal spiny neurons. *Stroke* **30**, 171–190.

Casali, T.A., Gomez, R.S., Moraes-Santos, T. & Gomez, M.V. 1995. Differential effects of calcium channel antagonists on tityustoxin and ouabain-induced release of [3H] acetylcholine from brain cortical slices. *Neuropharmacology* **34**, 599–603.

D'Ambrosio, R., Gordon, D.S. & Winn, H.R. 2002. Differential role of KIR channel and Na(+)/K(+)-pump in the regulation of extracellular K(+) in rat hippocampus. *J Neurophysiol* **87**, 87–102.

Dierkes, P.W., Wusten, H.J., Klees, G., Muller, A. & Hochstrate, P. 2006. Ionic mechanism of ouabian-induced swelling of leech Retzius neurons. *Pflugers Arch* **452**, 25–35.

Edward, C., Dolezal, D., Tucek, S., Zemkova, H. & Vyskocil, F. 1985. Is an acetylcholine transport system responsible for nonquantal release of acetycholine at the rodent myoneural junction? *Proc Natl Acad Sci USA* **82**, 3514–3518.

Gillis, R.A. & Quest, J.A. 1979. The role of the nervous system in the cardiovascular effects of digitalis. *Pharmacol Rev* **31**, 19–97.

Gomez, R.S., Gomez, M.V. & Prado, M.A.M. 1996. Inhibition of Na^+, K^+-ATPase by ouabain opens calcium channels coupled to acetylcholine release in guinea pig myenteric plexus. *J Neurochem* **66**, 1440–1447.

Haass, M., Serf, C., Gerber, S.H. *et al.* 1997. W. Dual effect of digitalis glycoside on norepinephrine release from human atrial tissue and bovine adrenal chromaffin cells: differential dependence on $[Na+]_i$ and $[Ca2+]_i$. *J Mol Cell Cardiol* **29**, 1615–1627.

Katsuragi, T., Ogawa, S. & Furukawa, T. 1994. Contribution of intra-and extracellular Ca^{2+} to noradrenaline exocytosis induced by ouabain and monesin from guinea-pig vas deferens. *Br J Pharmacol* **113**, 795–800.

Kawada, T., Yamazaki, T., Akiyama, T. *et al.* 2006. Effects of Ca2+ channel anatagonists on nerve stimulation-induced and ischemia-induced myocardial interstitial acetylcholine release in cats. *Am J Physiol* **291**, H2181–2191.

Kawada, T., Yamazaki, T., Akiyama, T. *et al.* 2001. *In vivo* assessment of acetylcholine-releasing function at cardiac vagal nerve terminals. *Am J Physiol* **281**, H139–H145.

Kranzhöfer, R., Haass, M., Kurz, T., Richardt, G. & Schömig, A. 1991. Effect of digitalis glycosides on norepinephrine release in the heart: dual mechanism of action. *Circ Res* **68**, 1628–1637.

Mclvor, M.E. & Cummings, C.C. 1987. Sodium fluoride produces a K+ efflux by increasing intracellular Ca2+ through Na+-Ca2+ exchange. *Toxicol Lett* **38**, 169–176.

Nikolsky, E.E., Voronin, V.A. & Vyskocil, F. 1991. Kinetic differences in the effect of calcium on quantal and non-quantal acetylcholine release at the murine diaphragm. *Neurosci Lett* **123**, 192–194.

Nishio, M., Ruch, S.W., Kelly, J.E., Aistrup, G.L., Sheehan, K. & Wasserstrom, J.A. 2004. Ouabain increases sarcoplasmic reticulum calcium release in cardiac myocytes. *J Pharmacol Exp Ther* **308**, 1181–1190.

Satoh, E. & Nakazato, Y. 1992. On the mechanisim of ouabain-induced release of acetylcholine from synaptsomes. *J Neurochem* **58**, 1038–1044.

Sharma, V.K., Pottick, L.A. & Banerjee, S.P. 1980. Ouabain stimulation of noradrenaline transport in guinea pig heart. *Nature* **286**, 817–819.

 doi: 10.1111/j.1748-1716.2007.01749.x

Smith, D.O. 1992. Routes of actylcholine leakage from cytosolic and vesicular compartments of rat motor nerve terminals. *Neurosci Lett* **135**, 5–9.

Sweadner, K. 1985. Ouabain-evoked norepinephrine release from intact rat sympathetic neurons: evidence for carrier-mediated release. *J Neurosci* **5**, 2397–2406.

Verbny, Y., Zhang, C.L. & Chiu, S.Y. 2002. Coupling of calcium homeostasis to axonal sodium in axons of mouse optic nerve. *J Neurophysiol* **88**, 802–816.

Vizi, E.S. 1998. Differential temperature dependence of carrier-mediated (cytoplasmic) and stimulus-evoked (exocytotic) release of transmitter: a simple method to separate two types of relase. *Neurochem Int* **33**, 359–366.

Vyskocil, F. & Illes, P. 1977. Non-quantal release of transmitter at mouse neuromuscular junction and its dependency on the activity of Na^+-K^+ ATPase. *Pflugers Arch* **370**, 295–297.

Wasserstrom, J.A. & Aistrup, G.L. 2005. Digitalis: new actions for an old drug. *Am J Physiol Heart Circ Physiol* **289**, H1781–H1793.

Wiedenkeller, D.E. & Sharp, G.W. 1984. Unexpected potentiation of insulin release by the calcium store blocker TMB-8. *Endocrinolgy* **114**, 116–119.

Yamazaki, T., Akiyama, T., Kitagawa, H., Takauchi, Y., Kawada, T. & Sunagawa, K. 1997. A new, concise dialysis approach to assessment of cardiac sympathetic nerve terminal abnormalities. *Am J Physiol* **272**, H1182–H1187.

Yamazaki, T., Akiyama, T., Kawada, T. *et al.* 1998. Norepinephrine efflux evoked by potassium chloride in cat sympathetic nerves: dual mechanism of action. *Brain Res* **794**, 146–150.

Yamazaki, T., Akiyama, T. & Mori, H. 2001. Effects of nociceptin on cardiac norepinephrine and acetylcholine release evoked by ouabain. *Brain Res* **904**, 153–156.

Zemkova, H., Vyskocil, F. & Edwards, C. 1990. The effect of nerve terminal activity on non-quantal release of acetylcholine at the mouse neuromuscular junction. *J Physiol* **423**, 631–640.

Am J Physiol Heart Circ Physiol 292: H921–H927, 2007.
First published September 29, 2006; doi:10.1152/ajpheart.00019.2006.

Evaluation of transmural distribution of viable muscle by myocardial strain profile and dobutamine stress echocardiography

Takeshi Maruo,[1] Satoshi Nakatani,[1] Yintie Jin,[2] Kazunori Uemura,[2] Masaru Sugimachi,[2] Hatsue Ueda-Ishibashi,[3] Masafumi Kitakaze,[1] Tohru Ohe,[4] Kenji Sunagawa,[2] and Kunio Miyatake[1]

Departments of [1]Cardiology and [3]Pathology, National Cardiovascular Center, and [2]Department of Cardiovascular Dynamics, National Cardiovascular Center Research Institute, Osaka, Japan; and [4]Department of Cardiovascular Medicine, Okayama University Graduate School of Medicine, Okayama, Japan

Submitted 5 January 2006; accepted in final form 27 September 2006

Maruo T, Nakatani S, Jin Y, Uemura K, Sugimachi M, Ueda-Ishibashi H, Kitakaze M, Ohe T, Sunagawa K, Miyatake K. Evaluation of transmural distribution of viable muscle by myocardial strain profile and dobutamine stress echocardiography. *Am J Physiol Heart Circ Physiol* 292: H921–H927, 2007. First published September 29, 2006; doi:10.1152/ajpheart.00019.2006.—Transmural distribution of viable myocardium in the ischemic myocardium has not been quantified and fully elucidated. To address this issue, we evaluated transmural myocardial strain profile (TMSP) in dogs with myocardial infarction using a newly developed tissue strain imaging. TMSP was obtained from the posterior wall at the epicardial left ventricular short-axis view in 13 anesthetized open-chest dogs. After control measurements, the left circumflex coronary artery was occluded for 90 min to induce subendocardial infarction (SMI). Subsequently, latex microbeads (90 μm) were injected in the same artery to create transmural infarction (TMI). In each stage, measurements were done before and after dobutamine challenge (10 $\mu g \cdot kg^{-1} \cdot min^{-1}$ for 10 min) to estimate transmural myocardial viability. Strain in the subendocardium in the control stage increased by dobutamine (from 53.6 ± 17.1 to 73.3 ± 21.8%, $P < 0.001$), whereas that in SMI and TMI stages was almost zero at baseline and did not increase significantly by dobutamine [from 0.8 ± 8.8 to 1.3 ± 7.0%, P = not significant (NS) for SMI, from −3.9 ± 5.6 to −1.9 ± 6.0%, P = NS for TMI]. Strain in the subepicardium increased by dobutamine in the control stage (from 23.9 ± 6.1 to 26.3 ± 6.4%, $P < 0.05$) and in the SMI stage (from 12.4 ± 7.3 to 27.1 ± 8.8%, $P < 0.005$), whereas that in the TMI stage did not change (from −1.0 ± 7.8 to −0.7 ± 8.3%, P = NS). In SMI, the subendocardial contraction was lost, but the subepicardium showed a significant increase in contraction with dobutamine. However, in TMI, even the subepicardial increase was not seen. Assessment of transmural strain profile using tissue strain imaging was a new and useful method to estimate transmural distribution of the viable myocardium in myocardial infarction.

myocardial infarction; strain; viability; echocardiography

IT IS WELL KNOWN that myocardial contraction has transmural heterogeneity. Several experimental studies confirmed that the subendocardium contributes greater to overall myocardial thickening than the subepicardium (6, 25). On the other hand, when a reduction of coronary blood flow occurs, a severe reduction of perfusion and kinesis occurs in the subendocardium, but only a trivial reduction can be detected in the subepicardium (5, 31). After a long period of ischemia, myocardial necrosis progresses from the endocardium to the epicardium (8, 13).

Myocardial strain reflects regional myocardial function. With the recent advancement of tissue Doppler echocardiography, myocardial strain can be obtained noninvasively (3, 33) and has been reported to be useful to quantify regional myocardial systolic function in ischemic heart disease (9, 11, 24, 29, 36). The recently developed myocardial strain imaging system provides us myocardial strain in each wall layer and shows its distribution in a form of transmural myocardial strain profile (TMSP; see Ref. 1). Thus combination of TMSP and dobutamine stress echocardiography (DSE), which has been used for the assessment of myocardial viability (18), is expected to demonstrate transmural distribution of viability. There have been no methods to visualize distribution of myocardial viability over the ventricular wall in myocardial infarction, and such method would provide important information in the clinical situation.

In the present study, to assess the transmural extent of myocardial infarction, we investigated TMSP in subendocardial and transmural myocardial infarction dog models and quantified the transmural heterogeneity of myocardial viability using myocardial strain imaging with DSE.

MATERIALS AND METHODS

Experimental subjects and settings. We used 13 mongrel dogs (weighing 27.3 ± 2.2 kg). After induction with intravenous pentobarbital sodium (25 mg/kg body wt), they were anesthetized with 2% isoflurane with oxygen. A median sternotomy was performed, the pericardium was split from apex to base, and, after the instrumentation, the edges of the pericardial incision were loosely resutured. A 5-Fr. micromanometer-tipped catheter (model MPC-500; Millar Instruments, Houston, TX) was positioned in the left ventricle through the apex to obtain peak systolic left ventricular pressure and peak positive and negative dP/d*t*. Electrocardiogram (ECG) was monitored from limb leads. Left ventricular pressure signals and ECG were digitized online. The care and use of animals was in strict accordance with the guiding principles of the American Physiological Society, and the experimental protocol was approved by the National Cardiovascular Center Committees on Animal Experiments.

Experimental protocol. A 6-Fr. sheath was placed in the right femoral artery, and an angioplasty balloon catheter was positioned in the proximal segment of the left circumflex coronary artery by the standard catheterization technique. DSE (dobutamine infusion at 10 $\mu g \cdot kg^{-1} \cdot min^{-1}$ for 10 min) was used to assess myocardial viability. At the control stage, echocardiographic and hemodynamic measurements were done before and after DSE. A subendocardial myocardial infarction was created by inflating the balloon for 90 min

Address for reprint requests and other correspondence: S. Nakatani, Dept. of Cardiology, National Cardiovascular Center, 5-7-1, Fujishiro-dai, Suita, Osaka 565-8565, Japan (e-mail: nakatas@hsp.ncvc.go.jp).

The costs of publication of this article were defrayed in part by the payment of page charges. The article must therefore be hereby marked "*advertisement*" in accordance with 18 U.S.C. Section 1734 solely to indicate this fact.

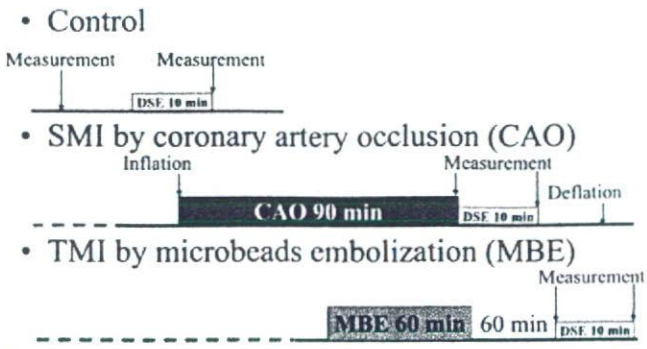

Fig. 1. Experimental protocol. DSE, dobutamine stress echocardiography; SMI, subendocardial myocardial infarction; TMI, transmural myocardial infarction.

(SMI stage; see Refs. 8 and 10), and DSE was performed during balloon inflation. After balloon deflation, 200–300 mg of latex microbeads (diameter 90 μm) were slowly injected in the same artery in 60 min to create a transmural myocardial infarction (TMI stage; see Refs. 7, 12, 15). At the TMI stage, DSE was performed 60 min after microbead embolization to complete myocardial infarction and to avoid ventricular instability to dobutamine challenge, and measurements were done before and after DSE (Fig. 1).

Ultrasound data acquisition. A commercially available ultrasound scanner (PowerVision 8000 3.5-MHz transducer; Toshiba, Tokyo, Japan) was used to obtain the epicardial left ventricular short-axis images at the level of basal and midventricle by tissue Doppler imaging. Recordings were stored in the form of digital loops of two cardiac cycles with 96–102 frames/s for subsequent analysis (33).

Tissue strain imaging. Strain is defined by the equation below and expresses the deformation of an object,

$$\text{Strain} = (L - L_0)/L_0$$

where L_0 is the length of an object before deformation and L is that after or during deformation. In echocardiography, L_0 is usually a muscle length at end diastole, and myocardial strain is used to express the deformation of local myocardial segments (4, 33).

In the present study, myocardial radial strain image was obtained from off-line analysis by using a research software TDI-Q (Toshiba; see Ref. 3). To obtain a strain image, TDI-Q software first calculates the myocardial displacement of all pixels of tissue by integrating myocardial velocity over a certain period. Because the frame rate was 96–102 frames/s, the step size for integration was 9.8–10.4 ms. Next, strain is obtained by evaluating the change of distance between pairs of two points defined on all pixels on the image by utilizing the displacement values. The distance of all two-pixel pairs at the initial time frame is equivalent to "L_0" on the above equation and set at 3 mm in this study (17). The initial time frame is set at end diastole to evaluate contraction; in other words "deformation" of the myocardium occurring in systole.

To measure local strain accurately, it is indispensable to obtain local velocity accurately. Therefore, the present myocardial strain imaging system has adopted tissue Doppler tracking and angle-correction techniques. Tissue Doppler tracking is an automatic motion tracking technique based on tissue Doppler information (30). By integrating a velocity of an indexed point on the ventricular wall known from tissue Doppler imaging, we can obtain myocardial displacement and predict the point where that point moves next. By repeating this procedure, the system can automatically track the motion of the point. With this technique, the influence of myocardial translation can be neglected. The angle-correction technique enables us to partly overcome the Doppler incident angle dependency that is inherent in Doppler echocardiography, as previous reports described (3, 26, 32). To correct the Doppler incident angle, a contraction center is set at the center of the left ventricular cavity at end systole in the left ventricular short-axis view. Next, the software automatically calculates the tissue velocity toward the contraction center (V_{motion}) by dividing the velocity toward a transducer (V_{beam}) by the cosine of the angle (θ) between the Doppler beam and the direction to the contraction center as follows:

$$V_{\text{motion}} = V_{\text{beam}}/\cos\theta$$

With the use of these two techniques, the research software TDI-Q automatically cancelled the effect of myocardial translation and angle dependency, accurately providing myocardial velocity, displacement, and strain (3). In the previously described experiments, the displacement data obtained by this method correlated with true displacement ($r = 0.99$, $P < 0.0001$; see Ref. 26).

Myocardial radial strain distribution over the myocardium is obtained as M-mode color-coded images, and the profile of distribution (TMSP) at end systole is shown as in Fig. 2. Bright color indicates high strain, and dark color indicates low strain. We obtained TMSP at basal and midinferolateral walls at end systole. We divided the myocardium into subendocardial and subepicardial half-layers by the midpoint of the myocardium at end systole. Mean strain values in the subendocardial half-layer and in the subepicardial half-layer were calculated by averaging strain values over each layer.

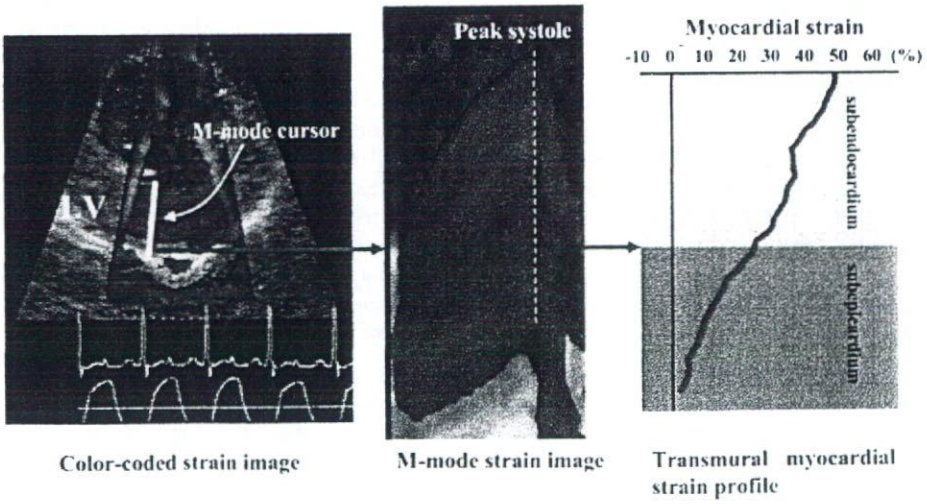

Fig. 2. Color-coded strain imaging, M-mode strain imaging, and transmural myocardial strain profile imaging in the control stage. *Left*: myocardial strain imaging of the left ventricular short axis at end systole. Red color means myocardial thickening. A white bar indicates an M-mode cursor. *Middle*: color-coded M-mode myocardial strain imaging obtained at the left ventricular posterior wall. The subendocardium is brighter than the subepicardium, indicating that the subendocardium contracts more vigorously. *Right*: transmural strain profile at end systole. The strain was highest at the subendocardium and lowest at the subepicardium, and the transmural strain showed a linear profile. LV, left ventricular wall.

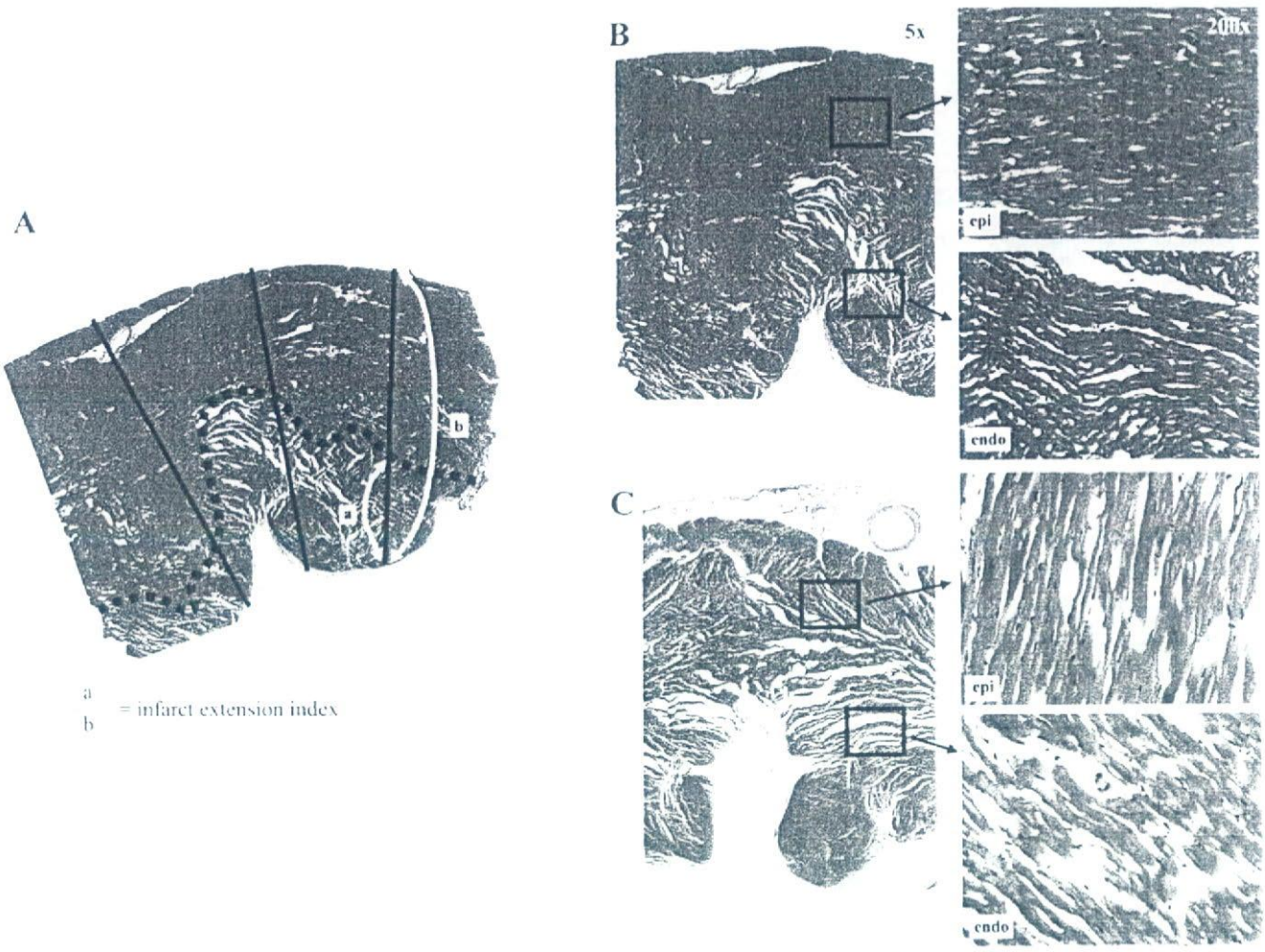

Fig. 3. *A*: determination of infarct extension index. Dotted line indicates the external limit of the infarcted zone. Examples of myocardial specimens taken after the SMI stage (*B*) and the TMI stage (*C*) stained by Masson's trichrome staining. In the SMI specimen, myocardial infarct was found only in the subendocardial layer, whereas acute ischemic changes such as wavy change or coagulation necrosis were recognized in both subendocardial and subepicardial layers in the TMI specimen. endo, Subendocardial layer; epi, subepicardial layer.

Histopathological studies. Establishment of subendocardial and transmural infarction by these techniques has been confirmed in our preliminary study and other previous studies (8, 10). We assessed the degree of extension of myocardial infarct also in the present study. At the end of the SMI stage in four dogs and the TMI stage in seven dogs, the heart was excised and cut into five to seven equally distant short-axis slices. Each slice was stained with hematoxylin-eosin and Masson's trichrome (Fig. 3). A pathologist who was blind to the experimental data examined the hearts histologically and measured the degree of infarct extension at the basal and midinferolateral walls, as previously reported (2). On each enlarged photomicrograph of the hearts, three to five transmural radii in the infarcted area were traced perpendicular to the endocardial and epicardial borders. The distance from the endocardial border to the external limit of the infarcted zone was measured and was expressed as a percentage of the distance between the endocardial and epicardial borders as an index of infarct extension, 100% being fully transmural and 0% being no infarction.

Table 1. *Hemodynamic parameters in control, SMI, and TMI stages*

	Baseline			DSE		
	Control (n = 13)	SMI (n = 11)	TMI (n = 7)	Control	SMI	TMI
HR, beats/min	133 ± 17	128 ± 27	129 ± 27	149 ± 22	134 ± 27	150 ± 19
LVP, mmHg	123 ± 10*†	108 ± 24	92 ± 21	136 ± 11†	132 ± 28†	112 ± 20
+dP/dt, mmHg/s	2,169 ± 484*†‡	1,577 ± 347*†	1,207 ± 279*	4,021 ± 979†‡	3,231 ± 844†	2,478 ± 1,138
−dP/dt, mmHg/s	−2,531 ± 408*†	−1,824 ± 606*†	−1,164 ± 465*	−3,188 ± 650†	−2,724 ± 892	−2,104 ± 526

Data are presented as means ± SD; n, no. of dogs. DSE, dobutamine stress echocardiography; SMI, subendocardial myocardial infarction; TMI, transmural myocardial infarction; HR, heart rate; LVP, peak systolic left ventricular pressure; +dP/dt, peak positive dP/dt; −dP/dt, peak negative dP/dt. $P < 0.05$ vs. DSE values (*), vs. SMI values (‡), and vs. TMI values (†).

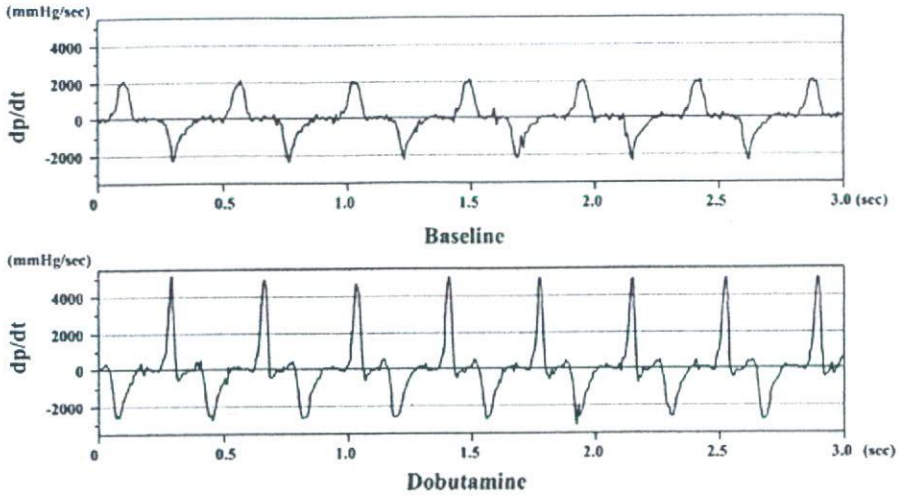

Fig. 4. dP/d*t* waveform before (*top*) and after (*bottom*) dobutamine infusion.

Reproducibility. Myocardial strain was measured by two independent observers and by one observer two times a week apart in 10 randomly selected segments to determine interobserver and intraobserver variability. The variability was assessed as the absolute difference between two measurements expressed as a percentage of their mean values. The interobserver variability was 6.5 ± 5.5 and 9.5 ± 7.5% for the subendocardial and subepicardial strains, respectively. The intraobserver variability was 7.2 ± 4.9 and 9.3 ± 3.7% for the subendocardial and subepicardial strains, respectively.

Statistical analysis. Hemodynamic data were obtained as an average of three to five consecutive beats. Statistical analyses were done with commercially available software (StatView 5.0; SAS Institute). Data are expressed as mean values ± SD. Comparisons of parameters among the stages were made by one-way ANOVA for repeated measures, followed by Scheffé's test. The Wilcoxon signed-ranks test was used to compare parameters before and after DSE. $P < 0.05$ was considered to indicate statistical significance.

RESULTS

Hemodynamic and histopathological data. Measurements were done in 13 dogs in the control stage, in 11 dogs in the SMI stage, and in 7 dogs in the TMI stage. Because of a large infarct created by the procedure, two dogs did not survive in the SMI stage and four dogs in the TMI stage. The absolute value of peak systolic left ventricular pressure and peak positive and negative dP/d*t* decreased gradually with the advancement of the stage. However, heart rate showed no significant changes. Both positive and negative dP/d*t* significantly increased in response to dobutamine administration (Table 1 and Fig. 4).

The degree of infarct extension was assessed at 14 sites from 4 dogs after the SMI stage and at 20 sites from 7 dogs after the TMI stage. The infarct extension index was 24.9 ± 7.8% for the SMI stage and 76.1 ± 9.9% for the TMI stage. Typical examples of the histopathological findings for both subendocardial and transmural infarcts are shown in Fig. 3.

Strain value in each stage. Myocardial strain was obtained at 25 segments in the control stage, at 20 segments in the SMI stage, and 11 segments in the TMI stage. Figure 5 shows representative TMSPs in each stage. In the control stage, myocardial strain was highest in the subendocardium and declined linearly toward the subepicardium. After DSE, TMSP

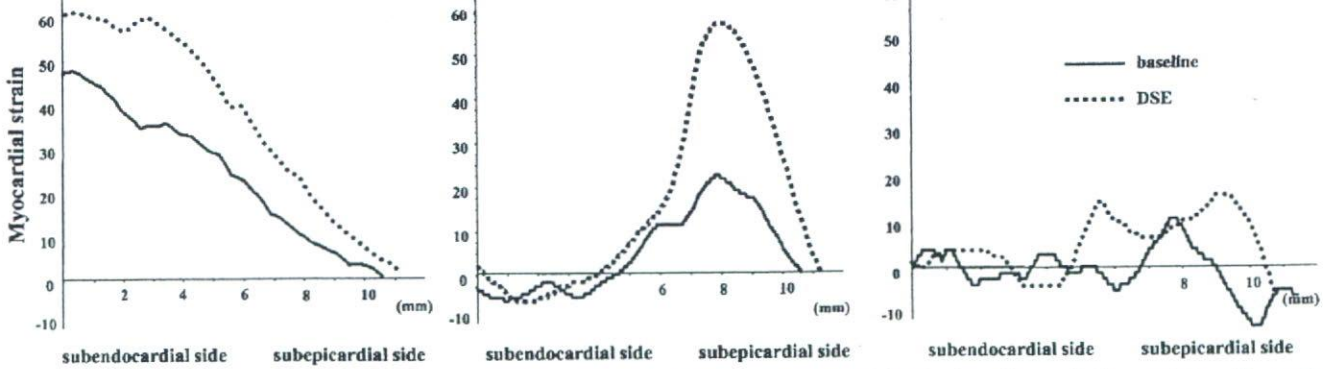

Fig. 5. Transmural myocardial strain profile before (solid lines) and after (dashed lines) dobutamine administration in each stage. *Left*: control stage. The profile was highest at the subendocardium and lowest at the subepicardium. With dobutamine administration, overall transmural myocardial strain increased. *Middle*: SMI stage. Myocardial strain at the subendocardium significantly decreased. With dobutamine administration, myocardial strain at the subepicardium showed a significant increase. *Right*: TMI stage. Overall transmural myocardial strain decreased at the baseline. Even after dobutamine administration, myocardial strain showed no significant increase.

Table 2. *Subendocardial and subepicardial strain in control, SMI, and TMI stages*

	Baseline			DSE		
	Control (n = 25)	SMI (n = 20)	TMI (n = 11)	Control	SMI	TMI
Endo strain	53.6±17.1*†‡	0.8±8.8	−3.9±5.6	73.3±21.8†‡	1.3±7.0	−1.9±6.0
Epi strain	23.9±6.1*†‡	12.4±7.3*†	−1.0±7.8	26.3±6.4†	27.1±8.8†	−0.7±8.3

Data are presented as means ± SD; n, no. of dogs. Endo strain, subendocardial strain; Epi strain, subepicardial strain. $P < 0.05$ vs. DSE values (*), vs. SMI values (‡), and vs. TMI values (†).

was uniformly uplifted, indicating the enhancement of contractility. In the SMI stage, subendocardial strain was almost zero before and after dobutamine challenge. In contrast, subepicardial strain increased after dobutamine, suggesting the presence of myocardial viability in the subepicardium. In the TMI stage, TMSP was almost flat before and after DSE, showing loss of myocardial viability through whole layers (Table 2).

Figure 6 shows changes in the subendocardial and subepicardial mean strain. Strain in the subendocardial half-layer was lower in the SMI and TMI stages than in the control stage (53.6 ± 17.1 vs. 0.8 ± 8.8 and −3.9 ± 5.6%, both $P < 0.001$).

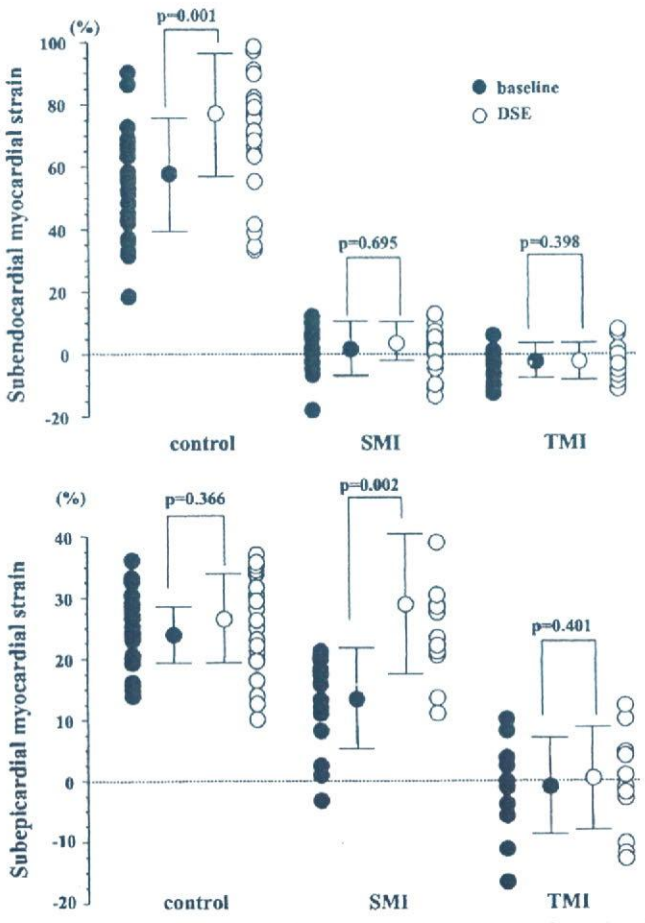

Fig. 6. Strain value in each layer. *Top*: subendocardial strain before (●) and after (○) dobutamine administration. Strain value in the subendocardial half-layer in the control stage increased with dobutamine, whereas that in the SMI and TMI stages showed no significant increase. *Bottom*: subepicardial strain before (●) and after (○) dobutamine administration. Strain value in the subepicardial half-layer in the SMI stage showed a significant increase. It showed no significant increase in the TMI stage.

There were no significant differences in the subendocardial strain between the SMI and TMI stages [P = not significant (NS)]. Strain in the subepicardial half-layer was lower in the TMI stage (−1.0 ± 7.8%) than that in the SMI stage (12.4 ± 7.3%, $P < 0.001$) and that in the control stage (23.9 ± 6.1%, $P < 0.001$).

Subendocardial strain in the control stage increased with DSE (53.6 ± 17.1 vs. 73.3 ± 21.8%, $P < 0.001$), whereas that in the SMI (0.8 ± 8.8 vs. 1.3 ± 7.0%, P = NS) and in the TMI stage (−3.9 ± 5.6 vs. −1.9 ± 6.0%, P = NS) showed no significant increase. Subepicardial strain in the control stage (23.9 ± 6.1 vs. 26.3 ± 6.4%, $P < 0.05$) and in the SMI stage (12.4 ± 7.3 vs. 27.1 ± 8.8%, $P < 0.005$) increased with DSE. It did not increase after DSE in the TMI stage (−1.0 ± 7.8 vs. −0.7 ± 8.3%, P = NS). Subepicardial strain after DSE showed no significant differences between the control and SMI stages (P = NS). These results showed that myocardial viability in the subepicardium was preserved in the SMI stage, whereas that in the TMI stage was lost.

DISCUSSION

In the present study, we analyzed the transmural distribution of viable muscle in myocardial infarction using echocardiography. Contraction in the subendocardium was lost and did not increase with dobutamine in either subendocardial infarction or transmural infarction models. On the other hand, subepicardial contraction was increased in subendocardial infarction but not in transmural infarction. These results showed that, with TMSP, we could quantify the transmural distribution of myocardial strain and identify the transmural differences in a local inotropic reserve in the viable and infarcted myocardium. The TMSP with DSE was useful to estimate the heterogeneity of transmural myocardial viability in SMI and TMI.

Transmural heterogeneity of myocardial viability. The left ventricular myocardium demonstrates transmural heterogeneity of strain distribution. It has been reported that, under normal circumstances, the subendocardial myocardium receives more blood flow and consumes more oxygen than the subepicardial one (20, 28, 35). Moreover, there is a transmural gradient of contractile function in the left ventricular wall, with greatest amount of thickening occurring in the subendocardial myocardium (6, 25). Clinically, these results were noninvasively confirmed in healthy subjects with tissue Doppler tracking technique (31). In the present study, strain value in the subendocardial layer was greater than that in the subepicardial layer in the control stage, being consistent with those of previous experimental and clinical studies. The linear decline pattern in TMSP was not observed in myocardial infarction. TMSP would potentially be useful for more detailed and innovative

evaluations of transmural myocardial function experimentally and clinically.

Effect of ischemia and dobutamine on transmural heterogeneity. After coronary artery occlusion, myocardial necrosis begins first in the endocardium and then progresses toward the epicardium with an increase in the occlusion time (8, 13). In our present study, we confirmed histologically that the SMI stage induced subendocardial infarction and the TMI stage induced transmural myocardial infarction. We observed continuous progression of myocardial dysfunction from the subendocardium to the subepicardium in myocardial infarction using echocardiography.

In acute animal models of reversible postischemic dysfunction and myocardial infarction, improved wall thickening during inotropic stimulation accurately differentiated reversible from fixed dysfunction and provided a better early assessment of viability than assessment of resting function alone (18). In clinical studies, contractile reserve by low-dose dobutamine was an independent predictor of functional recovery for myocardial infarction, which was superior to the other clinical criteria (23). In this experimental subendocardial infarction model, subendocardial strain showed no significant increase in response to inotropic stimulation, whereas subepicardial strain increased, indicating that the subepicardial myocardium was still viable. In the transmurally infarcted myocardium, myocardial strain of both subendocardium and subepicardium did not show significant increase. Therefore, the present method using TMSP and DSE is useful to visualize and quantify the contractile reserve and viability of both the subendocardium and the subepicardium.

Clinical implications. Because the prognosis of patients with subendocardial infarction is better than that with transmural infarction, assessment of the transmurality of myocardial necrosis and ischemia is an important clinical issue for patients with acute myocardial infarction or with chronic myocardial ischemia (22, 27). However, it has been difficult to make a diagnosis of subendocardial infarction by two-dimensional echocardiography. Some previous studies have shown that strain rate or strain echocardiography was useful to differentiate subendocardial infarction from transmural infarction (2, 34). We also obtained similar results using a new method of visualizing transmural myocardial strain distribution. Because the transmurality of necrosis is an important determinant of ultimate infarct size, its knowledge would be helpful in making therapeutic decisions for myocardial infarction (16, 34). Thus it is clinically helpful that we can quantify the transmural myocardial viability and necrosis extent. Furthermore, we could estimate the myocardial viability of each layer with DSE, enabling us to diagnose the stunned myocardium and predict myocardial functional recovery after myocardial infarction.

The present imaging system can be applied for the clinical evaluation of the various heart diseases characterized by subendocardial myocardial dysfunction such as anthracycline cardiotoxicity, syndrome X, hypertrophic cardiomyopathy, and dilated cardiomyopathy (14, 19, 21).

Study limitations. There was a possibility that some dogs in the subendocardial infarction models might develop transmural infarction. However, the 90-min ischemic period chosen for the subendocardial infarction models was similar to the previous studies, and it did result in subendocardial infarction (8, 10). In the present study, we showed histological evidence of subendocardial infarction after the SMI stage in parts of dogs. Furthermore, the difference in strain between the subendocardial and transmural infarction models was very prominent and consistent in each dog in the present study. These suggested that dogs after the SMI stage developed myocardial infarct almost only in the subendocardial layer.

We did not validate myocardial strain values using other methods, such as sonomicrometry. However, sonomicrometry is not always suitable to assess transmural distribution of myocardial strain, as shown in Fig. 5. We believe our measurement should be accurate because the displacement data obtained by our method were shown to be accurate (3, 21).

In conclusion, the quantitative analysis of transmural myocardial strain distribution could assess transmural differences in local inotropic reserve within the viable and infracted myocardium. In subendocardial infarction, the subepicardial myocardial strain showed an increase in contraction with dobutamine. However, in transmural infarction, this increase was lost. Assessment of transmural strain profile using tissue strain imaging was useful to quantify transmural distribution of the viable myocardium in SMI and TMI.

ACKNOWLEDGMENTS

We thank Yasuhiko Abe, Ryoichi Kanda, and Toshiba Corporation for providing research software assistance.

GRANTS

This work was partly supported by a Research Grant from the Ministry of Health, Labor and Welfare, Japan.

REFERENCES

1. **Chen X, Nakatani S, Hasegawa T, Maruo T, Kanzaki H, Miyatake K.** Effect of left ventricular systolic pressure on myocardial strain demonstrated by transmural myocardial strain profile. *Echocardiography* 23: 77–78, 2006.
2. **Derumeaux G, Loufoua J, Pontier G, Cribier A, Ovize M.** Tissue Doppler imaging differentiates transmural from nontransmural acute myocardial infarction after reperfusion therapy. *Circulation* 103: 589–596, 2001.
3. **Dohi K, Pinsky MR, Kanzaki H, Severyn D, Gorcsan J 3rd.** Effects of radial left ventricular dyssynchrony on cardiac performance using quantitative tissue Doppler radial strain imaging. *J Am Soc Echocardiogr* 19: 475–482, 2006.
4. **Edvardsen T, Gerber BL, Garot J, Bluemke DA, Lima JA, Smiseth OA.** Quantitative assessment of intrinsic regional myocardial deformation by Doppler strain rate echocardiography in humans: validation against three-dimensional tagged magnetic resonance imaging. *Circulation* 106: 50–56, 2002.
5. **Gallagher KP, Matsuzaki M, Koziol JA, Kemper WS, Ross J Jr.** Regional myocardial perfusion and wall thickening during ischemia in conscious dogs. *Am J Physiol Heart Circ Physiol* 247: H727–H738, 1984.
6. **Hartley CJ, Latson LA, Michael LH, Seidel CL, Lewis RM, Entman ML.** Doppler measurement of myocardial thickening with a single epicardial transducer. *Am J Physiol Heart Circ Physiol* 245: H1066–H1072, 1983.
7. **He KL, Dickstein M, Sabbah HN, Yi GH, Gu A, Maurer M, Wei CM, Wang J, Burkhoff D.** Mechanisms of heart failure with well preserved ejection fraction in dogs following limited coronary microembolization. *Cardiovasc Res* 64: 72–83, 2004.
8. **Homans DC, Pavek T, Laxson DD, Bache RJ.** Recovery of transmural and subepicardial wall thickening after subendocardial infarction. *J Am Coll Cardiol* 24: 1109–1116, 1994.
9. **Jamal F, Strotmann J, Weidemann F, Kukulski T, D'hooge J, Bijnens B, Van de Werf F, De Scheerder I, Sutherland GR.** Noninvasive quantification of the contractile reserve of stunned myocardium by ultrasonic strain rate and strain. *Circulation* 104: 1059–1065, 2001.
10. **Kim WG, Shin YC, Hwang SW, Lee C, Na CY.** Comparison of myocardial infarction with sequential ligation of the left anterior descend-

ing artery and its diagonal branch in dogs and sheep. *Int J Artif Organs* 26: 351–357, 2003.

11. **Kukulski T, Jamal F, Herbots L, D'hooge J, Bijnens B, Hatle L, De Scheerder I, Sutherland GR.** Identification of acutely ischemic myocardium using ultrasonic strain measurements. A clinical study in patients undergoing coronary angioplasty. *J Am Coll Cardiol* 41: 810–819, 2003.
12. **Lavine SJ, Prcevski P, Held AC, Johnson V.** Experimental model of chronic global left ventricular dysfunction secondary to left coronary microembolization. *J Am Coll Cardiol* 18: 1794–1803, 1991.
13. **Lowe JE, Cummings RG, Adams DH, Hull-Ryde EA.** Evidence that ischemic cell death begins in the subendocardium independent of variations in collateral flow or wall tension. *Circulation* 68: 190–202, 1983.
14. **Maier SE, Fischer SE, McKinnon GC, Hess OM, Krayenbuehl HP, Boesiger P.** Evaluation of left ventricular segmental wall motion in hypertrophic cardiomyopathy with myocardial tagging. *Circulation* 86: 1919–1928, 1992.
15. **Malyar NM, Lerman LO, Gossl M, Beighley PE, Ritman EL.** Relation of nonperfused myocardial volume and surface area to left ventricular performance in coronary microembolization. *Circulation* 110: 1946–1952, 2004.
16. **Mann DL, Gillam LD, Mich R, Foale R, Newell JB, Weyman AE.** Functional relation between infarct thickness and regional systolic function in the acutely and subacutely infarcted canine left ventricle. *J Am Coll Cardiol* 14: 481–488, 1989.
17. **Matre K, Fannelop T, Dahle GO, Heimdal A, Grong K.** Radial strain gradient across the normal myocardial wall in open-chest pigs measured with Doppler strain rate imaging. *J Am Soc Echocardiogr* 18: 1066–1073, 2005.
18. **Mercier JC, Lando U, Kanmatsuse K, Ninomiya K, Meerbaum S, Fishbein MC, Swan HJ, Ganz W.** Divergent effects of inotropic stimulation on the ischemic and severely depressed reperfused myocardium. *Circulation* 66: 397–400, 1982.
19. **Mortensen SA, Olsen HS, Baandrup U.** Chronic anthracycline cardiotoxicity: haemodynamic and histopathological manifestations suggesting a restrictive endomyocardial disease. *Br Heart J* 55: 274–282, 1986.
20. **Oh BH, Volpini M, Kambayashi M, Murata K, Rockman HA, Kassab GS, Ross J Jr.** Myocardial function and transmural blood flow during coronary venous retroperfusion in pigs. *Circulation* 86: 1265–1279, 1992.
21. **Panting JR, Gatehouse PD, Yang GZ, Grothues F, Firmin DN, Collins P, Pennell DJ.** Abnormal subendocardial perfusion in cardiac syndrome X detected by cardiovascular magnetic resonance imaging. *N Engl J Med* 346: 1948–1953, 2002.
22. **Picano E, Sicari R, Landi P, Cortigiani L, Bigi R, Coletta C, Galati A, Heyman J, Mattioli R, Previtali M, Mathias W Jr, Dodi C, Minardi G, Lowenstein J, Seveso G, Pingitore A, Salustri A, Raciti M.** Prognostic value of myocardial viability in medically treated patients with global left ventricular dysfunction early after an acute uncomplicated myocardial infarction: a dobutamine stress echocardiographic study. *Circulation* 98: 1078–1084, 1998.
23. **Pierard LA, De Landsheere CM, Berthe C, Rigo P, Kulbertus HE.** Identification of viable myocardium by echocardiography during dobutamine infusion in patients with myocardial infarction after thrombolytic therapy: comparison with positron emission tomography. *J Am Coll Cardiol* 15: 1021–1031, 1990.
24. **Pislaru C, Bruce CJ, Anagnostopoulos PC, Allen JL, Seward JB, Pellikka PA, Ritman EL, Greenleaf JF.** Ultrasound strain imaging of altered myocardial stiffness: stunned versus infarcted reperfused myocardium. *Circulation* 109: 2905–2910, 2004.
25. **Sabbah HN, Marzilli M, Stein PD.** The relative role of subendocardium and subepicardium in left ventricular mechanics. *Am J Physiol Heart Circ Physiol* 240: H920–H926, 1981.
26. **Sade LE, Severyn DA, Kanzaki H, Dohi K, Gorcsan J 3rd.** Second-generation tissue Doppler with angle-corrected color-coded wall displacement for quantitative assessment of regional left ventricular function. *Am J Cardiol* 92: 554–560, 2003.
27. **Sawada S, Bapat A, Vaz D, Weksler J, Fineberg N, Greene A, Gradus-Pizlo I, Feigenbaum H.** Incremental value of myocardial viability for prediction of long-term prognosis in surgically revascularized patients with left ventricular dysfunction. *J Am Coll Cardiol* 42: 2099–2105, 2003.
28. **Sjoquist PO, Duker G, Almgren O.** Distribution of the collateral blood flow at the lateral border of the ischemic myocardium after acute coronary occlusion in the pig and the dog. *Basic Res Cardiol* 79: 164–175, 1984.
29. **Skulstad H, Urheim S, Edvardsen T, Andersen K, Lyseggen E, Vartdal T, Ihlen H, Smiseth OA.** Grading of myocardial dysfunction by tissue Doppler echocardiography: a comparison between velocity, displacement, and strain imaging in acute ischemia. *J Am Coll Cardiol* 47: 1672–1682, 2006.
30. **Tanaka N, Tone T, Ono S, Tomochika Y, Murata K, Kawagishi T, Yamazaki N, Matsuzaki M.** Predominant inner-half wall thickening of left ventricle is attenuated in dilated cardiomyopathy: an application of tissue Doppler tracking technique. *J Am Soc Echocardiogr* 14: 97–103, 2001.
31. **Torry RJ, Myers JH, Adler AL, Liut CL, Gallagher KP.** Effects of nontransmural ischemia on inner and outer wall thickening in the canine left ventricle. *Am Heart J* 122: 1292–1299, 1991.
32. **Uematsu M, Miyatake K, Tanaka N, Matsuda H, Sano A, Yamazaki N, Hirama M, Yamagishi M.** Myocardial velocity gradient as a new indicator of regional left ventricular contraction: detection by a two-dimensional tissue Doppler imaging technique. *J Am Coll Cardiol* 26: 217–223, 1995.
33. **Urheim S, Edvardsen T, Torp H, Angelsen B, Smiseth OA.** Myocardial strain by Doppler echocardiography. Validation of a new method to quantify regional myocardial function. *Circulation* 102: 1158–1164, 2000.
34. **Weidemann F, Dommke C, Bijnens B, Claus P, D'hooge J, Mertens P, Verbeken E, Maes A, Van de Werf F, De Scheerder I, Sutherland GR.** Defining the transmurality of a chronic myocardial infarction by ultrasonic strain-rate imaging: implications for identifying intramural viability: an experimental study. *Circulation* 107: 883–888, 2003.
35. **Weiss HR, Neubauer JA, Lipp JA, Sinha AK.** Quantitative determination of regional oxygen consumption in the dog heart. *Circ Res* 42: 394–401, 1978.
36. **Williams RI, Payne N, Phillips T, D'hooge J, Fraser AG.** Strain rate imaging after dynamic stress provides objective evidence of persistent regional myocardial dysfunction in ischaemic myocardium: regional stunning identified? *Heart* 91: 152–160, 2005.

J Appl Physiol 102: 622–627, 2007.
First published November 2, 2006; doi:10.1152/japplphysiol.00622.2006.

Hypothermia reduces ischemia- and stimulation-induced myocardial interstitial norepinephrine and acetylcholine releases

Toru Kawada,[1] Hirotoshi Kitagawa,[2] Toji Yamazaki,[2] Tsuyoshi Akiyama,[2] Atsunori Kamiya,[1] Kazunori Uemura,[1] Hidezo Mori,[2] and Masaru Sugimachi[1]

[1]*Department of Cardiovascular Dynamics, Advanced Medical Engineering Center, and*
[2]*Department of Cardiac Physiology, National Cardiovascular Center Research Institute, Osaka, Japan*

Submitted 4 June 2006; accepted in final form 1 November 2006

Kawada T, Kitagawa H, Yamazaki T, Akiyama T, Kamiya A, Uemura K, Mori H, Sugimachi M. Hypothermia reduces ischemia- and stimulation-induced myocardial interstitial norepinephrine and acetylcholine releases. *J Appl Physiol* 102: 622–627, 2007. First published November 2, 2006; doi:10.1152/japplphysiol.00622.2006.—Although hypothermia is one of the most powerful modulators that can reduce ischemic injury, the effects of hypothermia on the function of the cardiac autonomic nerves in vivo are not well understood. We examined the effects of hypothermia on the myocardial interstitial norepinephrine (NE) and ACh releases in response to acute myocardial ischemia and to efferent sympathetic or vagal nerve stimulation in anesthetized cats. We induced acute myocardial ischemia by coronary artery occlusion. Compared with normothermia ($n = 8$), hypothermia at 33°C ($n = 6$) suppressed the ischemia-induced NE release [63 nM (SD 39) vs. 18 nM (SD 25), $P < 0.01$] and ACh release [11.6 nM (SD 7.6) vs. 2.4 nM (SD 1.3), $P < 0.01$] in the ischemic region. Under hypothermia, the coronary occlusion increased the ACh level from 0.67 nM (SD 0.44) to 6.0 nM (SD 6.0) ($P < 0.05$) and decreased the NE level from 0.63 nM (SD 0.19) to 0.40 nM (SD 0.25) ($P < 0.05$) in the nonischemic region. Hypothermia attenuated the nerve stimulation-induced NE release from 1.05 nM (SD 0.85) to 0.73 nM (SD 0.73) ($P < 0.05$, $n = 6$) and ACh release from 10.2 nM (SD 5.1) to 7.1 nM (SD 3.4) ($P < 0.05$, $n = 5$). In conclusion, hypothermia attenuated the ischemia-induced NE and ACh releases in the ischemic region. Moreover, hypothermia also attenuated the nerve stimulation-induced NE and ACh releases. The Bezold-Jarisch reflex evoked by the left anterior descending coronary artery occlusion, however, did not appear to be affected under hypothermia.

vagal nerve; sympathetic nerve; cardiac microdialysis; cats

HYPOTHERMIA IS ONE OF THE most powerful modulators that can reduce ischemic injury in the central nervous system, heart, and other organs. The general consensus is that hypothermia induces a hypometabolic state in tissues and balances energy supply and demand (25). With respect to the myocardial ischemia, the size of a myocardial infarction correlates with temperature (6), and mild hypothermia can protect the myocardium against acute ischemic injury (9). The effects of hypothermia on the function of the cardiac autonomic nerves in terms of neurotransmitter releases, however, are not fully understood. Because autonomic neurotransmitters such as norepinephrine (NE) and ACh directly impinge on the myocardium, they would be implicated in the cardioprotection by hypothermia.

In previous studies from our laboratory, Kitagawa et al. (16) demonstrated that hypothermia attenuated the nonexocytotic NE release induced pharmacologically by ouabain, tyramine, or cyanide. Kitagawa et al. (15) also demonstrated that hypothermia attenuated the exocytotic NE release in response to vena cava occlusion or to local administration of high K^+. The effects of hypothermia on the ischemia-induced myocardial interstitial NE release, however, were not examined in those studies. In addition, the effects of hypothermia on the ischemia-induced myocardial interstitial ACh release have never been examined. Because both sympathetic and parasympathetic nerves control the heart, simultaneous monitoring of the myocardial interstitial releases of NE and ACh (14, 31) would help integrative understanding of the autonomic nerve terminal function under hypothermia in conjunction with acute myocardial ischemia.

In the present study, the effects of hypothermia on the ischemia-induced and nerve stimulation-induced myocardial interstitial neurotransmitter releases were examined. We implanted a dialysis probe into the left ventricular free wall of anesthetized cats and measured dialysate NE and ACh levels as indexes of neurotransmitter outputs from the cardiac sympathetic and vagal nerve terminals, respectively. Based on our laboratory's previous results (15, 16), we hypothesized that hypothermia would attenuate the neurotransmitter releases in response to acute myocardial ischemia and to electrical nerve stimulation.

MATERIALS AND METHODS

Surgical Preparation and Protocols

Animals were cared for in accordance with the *Guiding Principles for the Care and Use of Animals in the Field of Physiological Sciences*, approved by the Physiological Society of Japan. All protocols were reviewed and approved by the Animal Subjects Committee of National Cardiovascular Center. Adult cats were anesthetized via an intraperitoneal injection of pentobarbital sodium (30–35 mg/kg) and ventilated mechanically through an endotracheal tube with oxygen-enriched room air. The level of anesthesia was maintained with a continuous intravenous infusion of pentobarbital sodium (1–2 $mg \cdot kg^{-1} \cdot h^{-1}$) through a catheter inserted from the right femoral vein. Mean arterial pressure (MAP) was measured using a pressure transducer connected to a catheter inserted from the right femoral artery. Heart rate (HR) was determined from an electrocardiogram.

Protocol 1: acute myocardial ischemia. We examined the effects of hypothermia on the ischemia-induced myocardial interstitial releases of NE and ACh. The heart was exposed by partially removing the left fifth and/or sixth rib. A dialysis probe was implanted transversely into

Address for reprint requests and other correspondence: T. Kawada, Dept. of Cardiovascular Dynamics, Advanced Medical Engineering Center, National Cardiovascular Center Research Institute, 5-7-1 Fujishirodai, Suita, Osaka 565-8565, Japan (e-mail: torukawa@res.ncvc.go.jp).

The costs of publication of this article were defrayed in part by the payment of page charges. The article must therefore be hereby marked "*advertisement*" in accordance with 18 U.S.C. Section 1734 solely to indicate this fact.

the anterolateral free wall of the left ventricle perfused by the left anterior descending coronary artery (LAD) to monitor myocardial interstitial NE and ACh levels in the ischemic region during occlusion of the LAD (13). Another dialysis probe was implanted transversely into the posterior free wall of the left ventricle perfused by the left circumflex coronary artery to monitor myocardial interstitial NE and ACh levels in a nonischemic region. Heparin sodium (100 U/kg) was administered intravenously to prevent blood coagulation. Animals were divided into a normothermic group (n = 8) and a hypothermic group (n = 6). In the hypothermic group, surface cooling with ice bags was performed until the esophageal temperature decreased to 33°C (15, 16). A stable hypothermic condition was obtained within ~2 h. In each group, we occluded the LAD for 60 min and examined changes in the myocardial interstitial NE and ACh levels in the ischemic region (i.e., the LAD region) and nonischemic region (i.e., the left circumflex coronary artery region). Fifteen-minute dialysate samples were obtained during the preocclusion baseline condition and during the periods of 0–15, 15–30, 30–45, and 45–60 min of the LAD occlusion.

Protocol 2: sympathetic stimulation. We examined the effects of hypothermia on the sympathetic nerve stimulation-induced myocardial interstitial NE release (n = 6). A dialysis probe was implanted transversely into the anterolateral free wall of the left ventricle. The bilateral cardiac sympathetic nerves originating from the stellate ganglia were exposed through a second intercostal space and sectioned. The cardiac end of each sectioned nerve was placed on a bipolar platinum electrode for sympathetic stimulation (5 Hz, 10 V, 1-ms pulse duration). The electrodes and nerves were covered with mineral oil to provide insulation and prevent desiccation. A 4-min dialysate sample was obtained during the sympathetic stimulation under the normothermic condition. Thereafter, hypothermia was introduced using the same cooling procedure as in *protocol 1*, and a second 4-min dialysate sample was obtained during the sympathetic stimulation.

Protocol 3: vagal stimulation. We examined the effects of hypothermia on the vagal nerve stimulation-induced ACh release (n = 5). A dialysis probe was implanted transversely into the anterolateral free wall of the left ventricle. The bilateral vagi were exposed through a midline cervical incision and sectioned at the neck. The cardiac end of each sectioned nerve was placed on a bipolar platinum electrode for vagal stimulation (20 Hz, 10 V, 1-ms pulse duration). To prevent severe bradycardia and cardiac arrest, which can be induced by the vagal stimulation, the heart was paced at 200 beats/min using pacing wires attached to the apex of the heart during the stimulation period. A 4-min dialysate sample was obtained during the vagal stimulation under the normothermic condition. Thereafter, hypothermia was introduced using the same cooling procedure as in *protocol 1*, and a second 4-min dialysate sample was obtained during the vagal stimulation.

Because of the relatively intense stimulation of the sympathetic or vagal nerve, the stimulation period in *protocols 2* and *3* was limited to 4 min to minimize gradual waning of the stimulation effects. At the end of the experiment, the animals were killed by increasing the depth of anesthesia with an overdose of pentobarbital sodium. We then confirmed that the dialysis probes had been threaded in the middle layer of the left ventricular myocardium.

Dialysis Technique

The dialysate NE and ACh concentrations were measured as indexes of myocardial interstitial NE and ACh levels, respectively. The materials and properties of the dialysis probe have been described previously (2, 3). Briefly, we designed a transverse dialysis probe. A dialysis fiber (13-mm length, 310-μm outer diameter, 200-μm inner diameter; PAN-1200, 50,000 molecular weight cutoff; Asahi Chemical) was connected at both ends to polyethylene tubes (25-cm length, 500-μm outer diameter, 200-μm inner diameter). The dialysis probe was perfused with Ringer solution containing a cholinesterase inhibitor eserine (10^{-4} M) at a rate of 2 μl/min. We started dialysate sampling from 2 h after the implantation of the dialysis probe(s), when the dialysate NE and ACh concentrations had reached steady states. The actual dialysate sampling was delayed by 5 min from the collection period to account for the dead space volume between the semipermeable membrane and the sample tube. Each sample was collected in a microtube containing 3 μl of HCl to prevent amine oxidation. The dialysate ACh concentration was measured directly by HPLC with electrochemical detection (Eicom). The in vitro recovery rate of ACh was ~70%. With the use of a criterion of signal-to-noise ratio of higher than three, the detection limit for ACh was 3 pg per injection. The dialysate NE concentration was measured by another HPLC-electrochemical detection system after the removal of interfering compounds by an alumina procedure. The in vitro recovery rate of NE was ~55%. With the use of a criterion of signal-to-noise ratio of higher than three, the detection limit for NE was 200 fg per injection.

Statistical Analysis

All data are presented as means and SD values. For *protocol 1*, we performed two-way repeated-measures ANOVA using hypothermia as one factor and the dialysate sampling periods (the effects of ischemia) as the other factor. For *protocols 2* and *3*, we compared stimulation-induced releases of NE and ACh before and during hypothermia using a paired t-test. For all of the statistics, the difference was considered significant when $P < 0.05$.

RESULTS

Figure 1*A* illustrates changes in myocardial interstitial NE levels in the ischemic region during LAD occlusion obtained from *protocol 1*. The *inset* shows the magnified ordinate for the

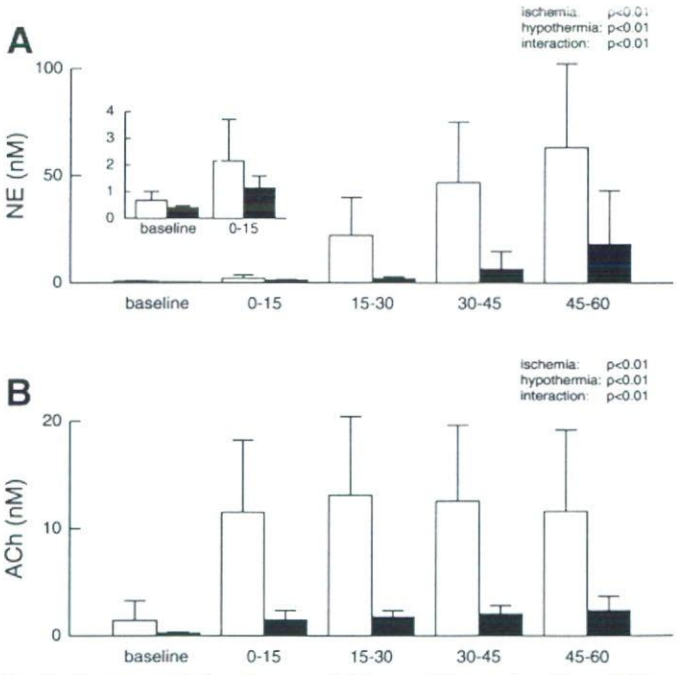

Fig. 1. *A*: ischemia-induced myocardial interstitial norepinephrine (NE) release in the ischemic region. Acute myocardial ischemia caused a progressive increase in the level of myocardial interstitial NE. Hypothermia attenuated the ischemia-induced NE release. *Inset*: magnified ordinate for the baseline and the 0- to 15-min period of ischemia. *B*: ischemia-induced myocardial interstitial ACh release in the ischemic region. Acute myocardial ischemia increased the myocardial interstitial ACh levels. Hypothermia attenuated the ischemia-induced ACh release. Open bars: normothermia; solid bars: hypothermia.

baseline and the 0- to 15-min period of ischemia. In the normothermic group (open bars), the LAD occlusion caused an ~94-fold increase in the NE level during the 45- to 60-min interval. In the hypothermic group (solid bars), the LAD occlusion caused an ~45-fold increase in the NE level during the 45- to 60-min interval. Compared with normothermia, hypothermia suppressed the baseline NE level to ~59% and the NE level during the 45- to 60-min period to ~29%. Statistical analysis indicated that the effects of both hypothermia and ischemia on the NE release were significant, and the interaction between hypothermia and ischemia was also significant.

Figure 1*B* illustrates changes in myocardial interstitial ACh levels in the ischemic region during the LAD occlusion. In both the normothermic (open bars) and hypothermic (solid bars) groups, the LAD occlusion caused an approximately eightfold increase in the ACh level during the 45- to 60-min interval. Compared with normothermia, however, hypothermia suppressed both the baseline ACh level and the ACh level during the 45- to 60-min period of ischemia to ~20%. Statistical analysis indicated that the effects of both hypothermia and ischemia on the ACh release were significant, and the interaction between hypothermia and ischemia was also significant.

Figure 2*A* illustrates changes in myocardial interstitial NE levels in the nonischemic region during the LAD occlusion. Note that scale of the ordinate is only one-hundredth of that in Fig. 1*A*. The LAD occlusion decreased the NE level in the normothermic group (open bars); the NE level during the 45- to 60-min interval was ~59% of the baseline level. The LAD occlusion also decreased the NE level in the hypothermic group (solid bars); the NE level during the 45- to 60-min interval was ~64% of the baseline level. Although the LAD occlusion resulted in a decrease in the NE level under both conditions, the NE level under hypothermia was nearly twice that measured under normothermia. The statistical analysis indicated that the effects of both hypothermia and ischemia on the NE release were significant, whereas the interaction between hypothermia and ischemia was not significant.

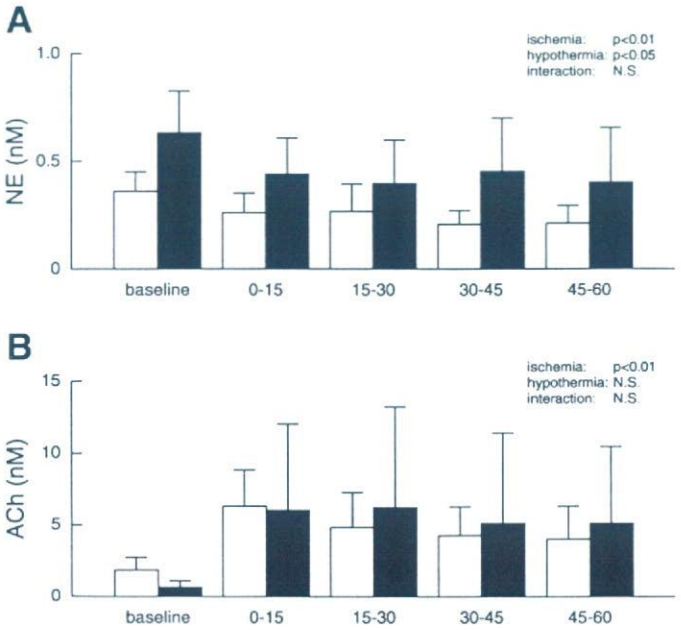

Fig. 2. *A*: changes in the myocardial interstitial NE levels in the nonischemic region. Acute myocardial ischemia decreased the level of myocardial interstitial NE from the baseline level. Hypothermia increased the myocardial interstitial NE levels in the nonischemic region. *B*: changes in the myocardial interstitial ACh levels in the nonischemic region. Acute myocardial ischemia increased the myocardial interstitial ACh level. Hypothermia did not attenuate the increasing response of ACh to the left anterior descending coronary artery occlusion. Open bars: normothermia; solid bars: hypothermia. NS, not significant.

Table 1. *Mean arterial pressure during acute myocardial ischemia obtained in protocol 1*

	Baseline	5 min	15 min	30 min	45 min	60 min
Normothermia	108 (23)	102 (28)	101 (24)	101 (20)	102 (21)	102 (21)
Hypothermia	108 (11)	80 (17)	87 (10)	85 (10)	86 (10)	91 (11)

Values are means (SD) (in mmHg) obtained during preocclusion baseline period and 5-, 15-, 30-, 45-, and 60-min periods of coronary artery occlusion. Ischemia: $P < 0.01$; hypothermia: not significant; interaction: $P < 0.01$.

Figure 2*B* illustrates changes in myocardial interstitial ACh levels in the nonischemic region during the LAD occlusion. The LAD occlusion caused an ~3.4-fold increase in the ACh level during the 0- to 15-min interval in the normothermic group (open bars). The LAD occlusion caused an approximately ninefold increase in the ACh level during the 0- to 15-min interval in the hypothermic group (solid bars). These effects of ischemia on the ACh release were statistically significant. Although hypothermia seemed to attenuate the baseline ACh level, the overall effects of hypothermia on the ACh level were insignificant.

Tables 1 and 2 summarize the MAP and HR data, respectively, obtained in *protocol 1*. Acute myocardial ischemia significantly reduced MAP ($P < 0.01$) and HR ($P < 0.01$). Hypothermia did not affect MAP but did decrease HR ($P < 0.01$). The interaction between ischemia and hypothermia was significant for MAP but not for HR by the two-way repeated-measures ANOVA.

For *protocol 2*, hypothermia significantly attenuated the sympathetic stimulation-induced NE release to ~70% of the level observed during normothermia (Fig. 3*A*). Under normothermia, the sympathetic stimulation increased MAP from 114 mmHg (SD 27) to 134 mmHg (SD 33) ($P < 0.01$) and HR from 147 beats/min (SD 9) to 207 beats/min (SD 5) ($P < 0.01$). Under hypothermia, the sympathetic stimulation increased MAP from 117 mmHg (SD 11) to 136 mmHg (SD 22) ($P < 0.05$) and HR from 125 beats/min (SD 16) to 164 beats/min (SD 10) ($P < 0.01$).

For *protocol 3*, hypothermia significantly attenuated the vagal stimulation-induced ACh release to ~70% of the level observed during normothermia (Fig. 3*B*). Hypothermia did not change MAP [117 mmHg (SD 18) vs. 118 mmHg (SD 27)] but

Table 2. *Heart rate during acute myocardial ischemia obtained in protocol 1*

	Baseline	5 min	15 min	30 min	45 min	60 min
Normothermia	183 (26)	160 (18)	163 (16)	163 (18)	166 (20)	165 (21)
Hypothermia	146 (25)	116 (19)	113 (19)	126 (39)	112 (20)	97 (31)

Values are means (SD) (in beats/min) obtained during preocclusion baseline period and 5-, 15-, 30-, 45-, and 60-min periods of coronary artery occlusion. Ischemia: $P < 0.01$; hypothermia: $P < 0.01$; interaction: not significant.

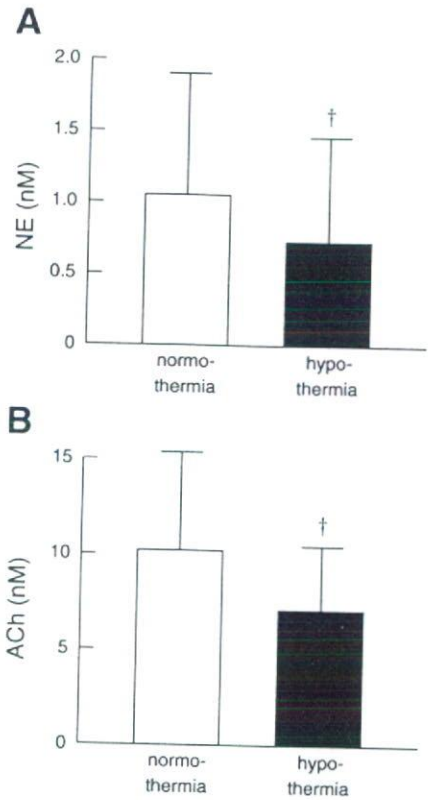

Fig. 3. *A*: efferent sympathetic nerve stimulation-induced release of myocardial interstitial NE before and during hypothermia. †Hypothermia significantly attenuated the stimulation-induced NE release. *B*: efferent vagal nerve stimulation-induced release of myocardial interstitial ACh before and during hypothermia. †Hypothermia significantly attenuated the stimulation-induced ACh release.

did decrease HR from 202 beats/min (SD 24) to 179 beats/min (SD 15) ($P < 0.05$) during the prestimulation, unpaced condition. MAP during the stimulation was 105 mmHg (SD 19) under normothermia and 93 mmHg (SD 33) under hypothermia.

DISCUSSION

A cardiac microdialysis is a powerful tool to estimate neurotransmitter levels in the myocardial interstitium in vivo (2, 3, 14, 19, 20, 31). The present study demonstrated that hypothermia significantly attenuated the myocardial interstitial releases of NE and ACh in the ischemic region during the LAD occlusion. In contrast, the increasing response in the ACh level from its baseline level and the decreasing response in the NE level from its baseline level observed in the nonischemic region were maintained under hypothermia. To our knowledge, this is the first report showing the effects of hypothermia on the myocardial interstitial releases of NE and ACh during acute myocardial ischemia in vivo. In addition, the present study showed that hypothermia significantly attenuated nerve stimulation-induced myocardial interstitial NE and ACh releases in vivo.

Effects of Hypothermia on Ischemia-induced NE and ACh Releases in the Ischemic Region

Acute myocardial ischemia causes energy depletion, which leads to myocardial interstitial NE release in the ischemic region (Fig. 1*A*). The NE release can be classified as exocytotic or nonexocytotic (18, 24). Exocytotic release indicates NE release from synaptic vesicles, which normally occurs in response to nerve discharge and subsequent Ca^{2+} influx through voltage-dependent Ca^{2+} channels. On the other hand, nonexocytotic release indicates NE release from the axoplasm, such as that mediated by a reverse transport through the NE transporter. A neuronal uptake blocker, desipramine, can suppress the ischemia-induced NE release (19, 24). Whereas exocytotic release contributes to the ischemia-induced NE release in the initial phase of ischemia (within ~20 min), carrier-mediated nonexocytotic release becomes predominant as the ischemic period is prolonged (1). Hypothermia significantly attenuated the ischemia-induced NE release (Fig. 1*A*). The NE level during the 45- to 60-min period of ischemia under hypothermia was ~20% of that obtained under normothermia. The NE uptake transporter is driven by the Na^+ gradient across the cell membrane (23). The loss of the Na^+ gradient due to ischemia causes NE to be transported out of the cell by reversing the action of the NE transporter. Hypothermia inhibits the action of the NE transporter and also suppresses the intracellular Na^+ accumulation (8), thereby reducing nonexocytotic NE release during ischemia. The present results are in line with an in vitro study that showed hypothermia suppressed nonexocytotic NE release induced by deprivation of oxygen and glucose (30). The present results are also consistent with a previous study from our laboratory that showed hypothermia attenuated the nonexocytotic NE release induced by ouabain, tyramine, or cyanide (16).

Acute myocardial ischemia increases myocardial interstitial ACh level in the ischemic region, as reported previously (Fig. 1*B*) (13). The level of ischemia-induced ACh release during 0- to 15-, 15- to 30-, 30- to 45-, or 45- to 60-min period of ischemia is comparable to that evoked by 4-min electrical stimulation of the bilateral vagi (Fig. 3*B*). Compared with the normothermic condition, hypothermia significantly attenuated the ischemia-induced myocardial interstitial release of ACh in the ischemic region. Our laboratory's previous study indicated that intracellular Ca^{2+} mobilization is essential for the ischemia-induced release of ACh (13). Hypothermia may have prevented the Ca^{2+} overload, thereby reducing the ischemia-induced ACh release. Alternatively, hypothermia may reduce the extent of the ischemic injury, which in turn suppressed the ischemia-induced ACh release. Because ACh has protective effects on the cardiomyocytes against ischemia (11), the suppression of ischemia-induced ACh release during hypothermia itself may be unfavorable for cardioprotection.

There is considerable controversy regarding the cardioprotective effects of β-adrenergic blockade during severe ischemia, with studies demonstrating a reduction of infarct size (10, 17) or no effects (7, 27). The β-adrenergic blockade seems effective to protect the heart only when the heart is reperfused within a certain period after the coronary occlusion. The β-adrenergic blockade would reduce the myocardial oxygen consumption through the reduction of HR and ventricular contractility and delay the progression of ischemic injury. Hence the infarct size might be reduced when the heart is reperfused before the ischemic damage becomes irreversible. The ischemia-induced NE release reached nearly 100 times the baseline NE level under normothermia (Fig. 1*A*), which by far exceeded the NE level attained by electrical stimulation of the

bilateral stellate ganglia (Fig. 3*A*). Because high NE levels have cardiotoxic effects (22), ischemia-induced NE release might aggravate the ischemic injury. However, catecholamine depletion by a reserpine treatment fails to reduce the infarct size (26, 29), throwing a doubt on the involvement of catecholamine toxicity in the progression of myocardial damage during ischemia. It is, therefore, most likely that the hypothermia-induced reductions in NE and ACh are the result of reduced myocardial damage or a direct effect on nerve endings.

Van den Doel et al. (28) showed that hypothermia does not abolish necrosis, but rather delays necrosis during sustained ischemia, so that hypothermia protected against infarction produced by a 30-min occlusion but not against infarction produced by a 60-min occlusion in the rat heart. At the same time, they mentioned that hypothermia was able to reduce the infarct size after a 60-min coronary occlusion in the dog, possibly because of the significant collateral flow in the canine hearts. Because the feline hearts are similar to the canine hearts in that they have considerable collateral flow compared with the rat hearts (21), hypothermia should have protected the feline heart against the 60-min coronary occlusion in the present study.

Effects of Hypothermia on the NE and ACh Releases in the Nonischemic Region and on the Electrical Stimulation-induced NE and ACh Releases

The NE and ACh levels in the nonischemic region may reflect the sympathetic and parasympathetic drives to this region. As an example, myocardial interstitial ACh levels increase during activations of the arterial baroreflex and the Bezold-Jarisch reflex (14). In the present study, acute myocardial ischemia decreased the NE level from its baseline level, whereas it increased the ACh level from its baseline level (Fig. 2). Ischemia also decreased MAP and HR (Tables 1 and 2), suggesting that the Bezold-Jarisch reflex was induced by the LAD occlusion under both normothermia and hypothermia. Taking into account the fact that electrical stimulation-induced ACh release was attenuated to ~70% (Fig. 3), similar ACh levels during ischemia imply the enhancement of the parasympathetic outflow via the Bezold-Jarisch reflex under hypothermia. These results are in line with the study by Zheng et al. (32), where pulmonary chemoreflex-induced bradycardia was maintained under hypothermia. Hypothermia increased the NE level in the nonischemic region, suggesting that sympathetic drive to this region also increased. Hypothermic stress is known to cause sympathetic activation, accompanying increases in MAP, HR, plasma NE, and epinephrine levels (4). In the present study, because the effect of hypothermia on MAP was insignificant (Table 1) and HR decreased under hypothermia (Table 2), the sympathetic activation observed in the nonischemic region might have been regional and not systemic.

Hypothermia attenuated the releases of NE and ACh in response to respective nerve stimulation to ~70% of that observed under normothermia (Fig. 3). The suppression of the exocytotic NE release by hypothermia is consistent with a previous study from our laboratory, where hypothermia attenuated the myocardial interstitial NE release in response to vena cava occlusion or to a local high K^+ administration (15). The suppression of NE release by hypothermia is consistent with an in vitro study by Kao and Westhead (12) in which catecholamine secretion from adrenal chromaffin cells induced by elevated K^+ levels increased as the temperature increased from 4 to 37°C. On the other hand, because hypothermia inhibits the neuronal NE uptake, the NE concentration at the synaptic cleft is expected to be increased if the level of NE release remains unchanged. Actually, Vizi (30) demonstrated that hypothermia increased NE release in response to field stimulation in vitro. In the present study, however, the suppression of NE release might have canceled the potential accumulation of NE due to NE uptake inhibition. The present study also demonstrated that the ACh release was suppressed by hypothermia. In the rat striatum, hypothermia decreases the extracellular ACh concentration and increases the choline concentration (5). Hypothermia may inhibit a choline uptake transporter in the same manner as it inhibits a NE uptake transporter. The inhibition of the choline transporter by hypothermia may have hampered the replenishment of the available pool of ACh and thereby contributed to the suppression of the stimulation-induced ACh release.

Limitations

In *protocol 1*, because we did not measure the infarct size in the present study, the degree of myocardial protection by hypothermia was undetermined. Whether the reduction of ischemia-induced neurotransmitter release correlates with the reduction of infact size requires further investigations. In *protocols 2* and *3*, baseline NE and ACh levels were not measured. The reduction of stimulation-induced NE and ACh release by hypothermia might be partly due to the reduction of baseline NE and ACh levels. However, because transection of the stellate ganglia (31) or vagi (3) reduces the baseline NE and ACh levels, changes in the baseline NE and ACh levels by hypothermia in *protocols 2* and *3* could not be as large as those observed under innervated conditions in *protocol 1* (Figs. 1 and 2).

In conclusion, hypothermia attenuated the ischemia-induced releases of NE and ACh in the ischemic region to ~30 and 20% of those observed under normothermia, respectively. Hypothermia also attenuated the nerve stimulation-induced releases of NE and ACh to ~70% of those observed during normothermia. In contrast, hypothermia did not affect the decreasing response in the NE level and the increasing response in the ACh level in the nonischemic region, suggesting that the Bezold-Jarisch reflex evoked by the LAD occlusion was maintained.

GRANTS

This study was supported by Health and Labour Sciences Research Grant for Research on Advanced Medical Technology, Health and Labour Sciences Research Grant for Research on Medical Devices for Analyzing, Supporting and Substituting the Function of Human Body, and Health and Labour Sciences Research Grant H18-Iryo-Ippan-023 from the Ministry of Health, Labour and Welfare of Japan; Program for Promotion of Fundamental Studies in Health Science from the National Institute of Biomedical Innovation; a grant provided by the Ichiro Kanehara Foundation; Ground-based Research Announcement for Space Utilization promoted by the Japan Space Forum; and Industrial Technology Research Grant Program 03A47075 from the New Energy and Industrial Technology Development Organization of Japan.

REFERENCES

1. **Akiyama T, Yamazaki T.** Norepinephrine release from cardiac sympathetic nerve endings in the in vivo ischemic region. *J Cardiovasc Pharmacol* 34: S11–S14, 1999.

2. **Akiyama T, Yamazaki T, Ninomiya I.** In vivo monitoring of myocardial interstitial norepinephrine by dialysis technique. *Am J Physiol Heart Circ Physiol* 261: H1643–H1647, 1991.
3. **Akiyama T, Yamazaki T, Ninomiya I.** In vivo detection of endogenous acetylcholine release in cat ventricles. *Am J Physiol Heart Circ Physiol* 266: H854–H860, 1994.
4. **Chernow B, Lake CR, Zaritsky A, Finton CK, Casey L, Rainey TG, Fletcher JR.** Sympathetic nervous system "switch off" with severe hypothermia. *Crit Care Med* 11: 677–680, 1983.
5. **Damsma G, Fibiger HC.** The effects of anaesthesia and hypothermia on interstitial concentrations of acetylcholine and choline in rat striatum. *Life Sci* 48: 2469–2474, 1991.
6. **Duncker DJ, Klassen CL, Ishibashi Y, Herrlinger SH, Pavek T, Bache R.** Effect of temperature on myocardial infarction in swine. *Am J Physiol Heart Circ Physiol* 270: H1189–H1199, 1996.
7. **Genth K, Hofmann M, Hofmann M, Schaper W.** The effect of β-adrenergic blockade on infarct size following experimental coronary occlusion. *Basic Res Cardiol* 76: 144–151, 1981.
8. **Gerevich Z, Tretter L, Adam-Vizi V, Baranyi M, Kiss JP, Zelles T, Vizi ES.** Analysis of high intracellular [Na^+]-induced release of [^{3}H]noradrenaline in rat hippocampal slices. *Neuroscience* 104: 761–768, 2001.
9. **Hale SL, Kloner RA.** Myocardial temperature in acute myocardial infarction: protection with mild regional hypothermia. *Am J Physiol Heart Circ Physiol* 273: H220–H227, 1997.
10. **Jang IK, Van de Werf F, Vanhaecke J, De Geest H.** Coronary reperfusion by thrombolysis and early beta-adrenergic blockade in acute experimental myocardial infarction. *J Am Coll Cardiol* 14: 1816–1823, 1989.
11. **Kakinuma Y, Ando M, Kuwabara M, Katare RG, Okudela K, Kobayashi M, Sato T.** Acetylcholine from vagal stimulation protects cardiomyocytes against ischemia and hypoxia involving additive nonhypoxic induction of HIF-1α. *FEBS Lett* 579: 2111–2118, 2005.
12. **Kao LS, Westhead EW.** Temperature dependence of catecholamine secretion from cultured bovine chromaffin cells. *J Neurochem* 43: 590–592, 1984.
13. **Kawada T, Yamazaki T, Akiyama T, Sato T, Shishido T, Inagaki M, Takaki H, Sugimachi M, Sunagawa K.** Differential acetylcholine release mechanisms in the ischemic and non-ischemic myocardium. *J Mol Cell Cardiol* 32: 405–414, 2000.
14. **Kawada T, Yamazaki T, Akiyama T, Shishido T, Inagaki M, Uemura K, Miyamoto T, Sugimachi M, Takaki H, Sunagawa K.** In vivo assessment of acetylcholine-releasing function at cardiac vagal nerve terminals. *Am J Physiol Heart Circ Physiol* 281: H139–H145, 2001.
15. **Kitagawa H, Akiyama T, Yamazaki T.** Effects of moderate hypothermia on in situ cardiac sympathetic nerve endings. *Neurochem Int* 40: 235–242, 2002.
16. **Kitagawa H, Yamazaki T, Akiyama T, Mori H, Sunagawa K.** Effects of moderate hypothermia on norepinephrine release evoked by ouabain, tyramine and cyanide. *J Cardiovasc Pharmacol* 41: S111–S114, 2003.
17. **Ku DD, Lucchesi BR.** Effects of dimethyl propranolol (UM-272; SC-27761) on myocardial ischemic injury in the canine heart after temporary coronary artery occlusion. *Circulation* 57: 541–548, 1978.
18. **Kurz T, Richardt G, Hagl S, Seyfarth M, Schömig A.** Two different mechanisms of noradrenaline release during normoxia and simulated ischemia in human cardiac tissue. *J Mol Cell Cardiol* 27: 1161–1172, 1995.
19. **Lameris TW, de Zeeuw S, Alberts G, Boomsma F, Duncker DJ, Verdouw PD, Veld AJ, van den Meiracker AH.** Time course and mechanism of myocardial catecholamine release during transient ischemia in vivo. *Circulation* 101: 2645–2650, 2000.
20. **Lameris TW, de Zeeuw S, Duncker DJ, Alberts G, Boomsma F, Verdouw PD, van den Meiracker AH.** Exogenous angiotensin II does not facilitate norepinephrine release in the heart. *Hypertension* 40: 491–497, 2002.
21. **Maxwell MP, Hearse DJ, Yellon DM.** Species variation in the coronary collateral circulation during regional myocardial ischaemia: a critical determinant of the rate of evolution and extent of myocardial infarction. *Cardiovasc Res* 21: 737–746, 1987.
22. **Rona G.** Catecholamine cardiotoxicity. *J Mol Cell Cardiol* 17: 291–306, 1985.
23. **Schwartz JH.** Neurotransmitters. In: *Principles of Neural Science* (4th Ed.), edited by Kandel ER, Schwartz JH, Jessell TM. New York: McGraw-Hill, 2000, p. 280–297.
24. **Schömig A, Kurz T, Richardt G, Schömig E.** Neuronal sodium homeostasis and axoplasmic amine concentration determine calcium-independent noradrenaline release in normoxic and ischemic rat heart. *Circ Res* 63: 214–226, 1988.
25. **Simkhovich BZ, Hale SL, Kloner RA.** Metabolic mechanism by which mild regional hypothermia preserves ischemic tissue. *J Cardiovasc Pharmacol Ther* 9: 83–90, 2004.
26. **Toombs CF, Wiltse AL, Shebuski RJ.** Ischemic preconditioning fails to limit infarct size in reserpinized rabbit myocardium. Implication of norepinephrine release in the preconditioning effect. *Circulation* 88: 2351–2358, 1993.
27. **Torr S, Drake-Holland AJ, Main M, Hynd J, Isted K, Noble MIM.** Effects on infarct size of reperfusion and pretreatment with β-blockade and calcium antagonists. *Basic Res Cardiol* 84: 564–582, 1989.
28. **Van den Doel MA, Gho BC, Duval SY, Schoemaker RG, Duncker DJ, Verdouw PD.** Hypothermia extends the cardioprotection by ischaemic preconditioning to coronary artery occlusions of longer duration. *Cardiovasc Res* 37: 76–81, 1998.
29. **Vander Heide RS, Schwartz LM, Jennings RB, Reimer KA.** Effect of catecholamine depletion on myocardial infarct size in dogs: role of catecholamines in ischemic preconditioning. *Cardiovasc Res* 30: 656–662, 1995.
30. **Vizi ES.** Different temperature dependence of carrier-mediated (cytoplasmic) and stimulus-evoked (exocytotic) release of transmitter: a simple method to separate the two types of release. *Neurochem Int* 33: 359–366, 1998.
31. **Yamazaki T, Akiyama T, Kitagawa H, Takauchi Y, Kawada T, Sunagawa K.** A new, concise dialysis approach to assessment of cardiac sympathetic nerve terminal abnormalities. *Am J Physiol Heart Circ Physiol* 272: H1182–H1187, 1997.
32. **Zheng F, Kidd C, Bowser-Riley F.** Effects of moderate hypothermia on baroreflex and pulmonary chemoreflex heart rate response in decerebrate ferrets. *Exp Physiol* 81: 409–420, 1996.